

- 7. Testing Flat Surface Optical Components
 - 7.1 Mirrors
 - 7.1.1 Fizeau Interferometer
 - 7.1.2 Twyman-Green Interferometer
 - 7.1.3 Ritchey-Common Test
 - 7.1.4 Naked Eye Test
 - 7.2 Windows
 - 7.2.1 Interferometer
 - 7.2.2 Autocollimator
 - 7.3 Prisms
 - 7.3.1 Interferometer
 - 7.3.2 Goniometer
 - 7.3.3 Autocollimator
 - 7.3.4 Naked Eye Tests
 - 7.4 Corner Cubes
 - 7.5 Diffraction Gratings
 - 7.6 Index inhomogeneity

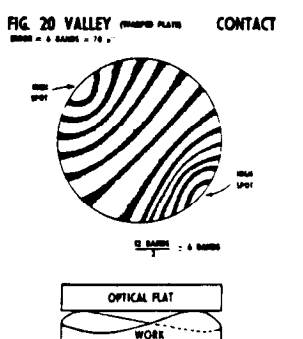
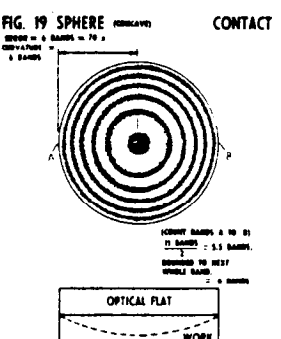
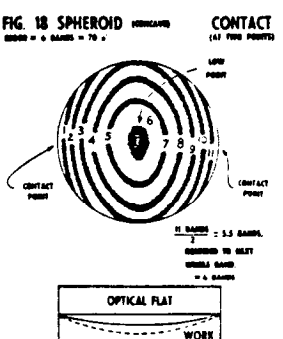
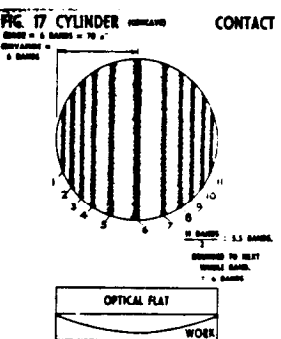
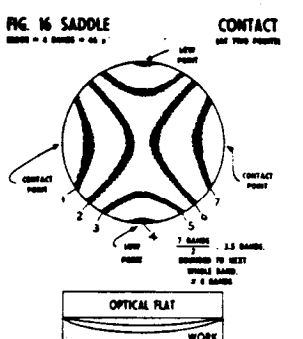
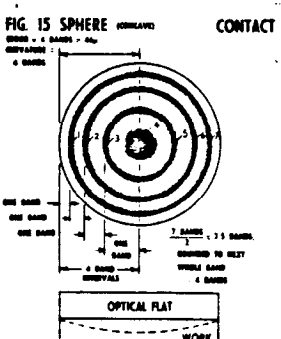
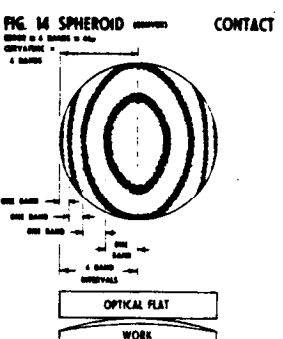
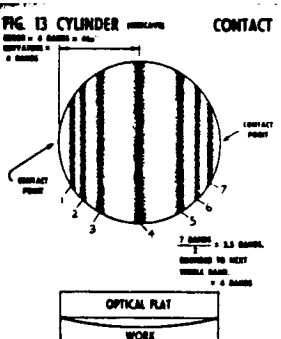
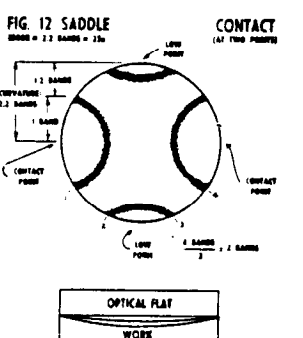
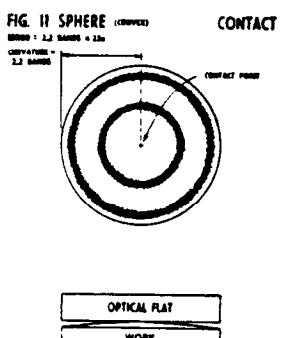
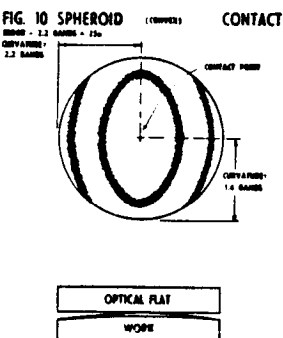
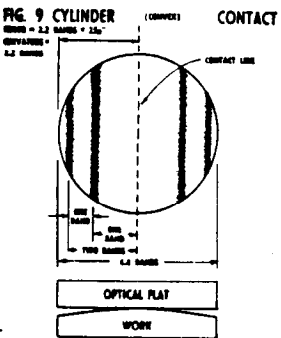
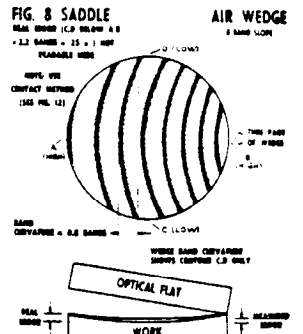
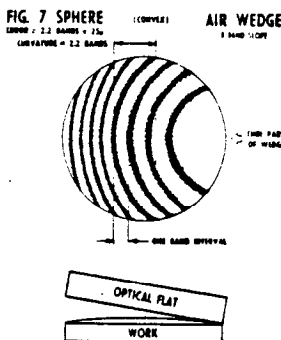
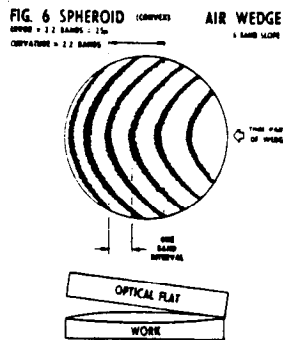
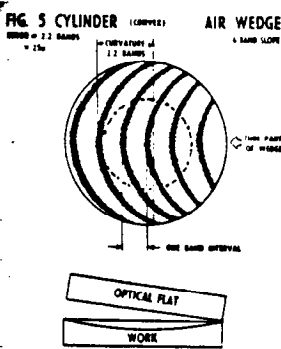
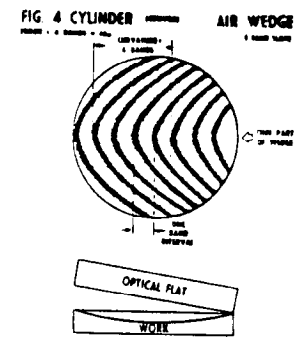
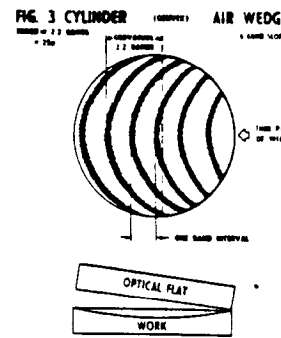
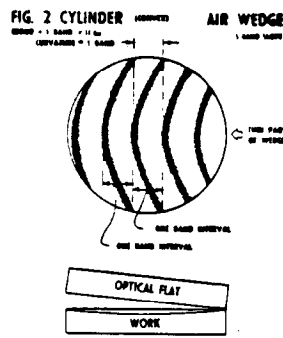
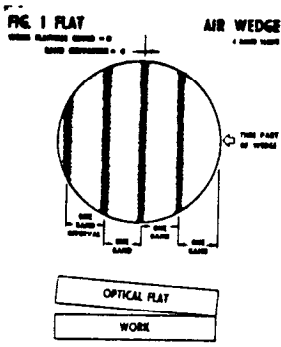
7.1 Mirrors

An interferometer is generally used to measure surface flatness. The best interferometer for a particular measurement depends upon the equipment available and the size of the sample being tested. The simplest interferometer for many surface flatness measurements is the Fizeau interferometer.

7.1.1 Fizeau Interferometer

The basic use of a Fizeau interferometer for measuring the surface height differences between two surfaces was described earlier. If the reference surface is flat, then surface flatness is being measured. The figure shows several Fizeau interferograms with various types and magnitudes of defects. The drawings were obtained from the Van Keuren Co.

It should be noted that even if two surfaces match for various rotations and translations, the two surfaces need not be flat; the two surfaces could be spherical, where one is convex and the second is concave. To be sure the surfaces are indeed flat, three surfaces are required, where the interference between any two gives straight equi-spaced fringes.



the pinhole. To facilitate preliminary adjustment, the screen is used to project the two pinhole images from the two reflecting plane surfaces. This is accomplished by removing the negative lens between the beam divider and the ground-glass screen. The pinhole image from the reference surface is at the center of the screen, whereas the one from the surface under test is somewhere on the screen; by manipulation of this surface, the two spots of light on the screen can be brought into coincidence. Then the negative lens is inserted in the path, and the Fizeau fringes are projected on the screen. These fringes can be further adjusted in direction and number as required. By the use of another beam divider, it is possible to divert part of the beam to a camera for taking a photograph of the fringe pattern. The whole instrument must be mounted on a suitable vibration-isolated platform.

This instrument can be used for various other applications that are normally not possible with conventional sources of light. We describe some such applications in the sections that follow. In addition, many possibilities exist for other applications, depending on the particular situations involved.

Several commercial Fizeau interferometers have been available for several years, but probably the two most widely known are the Zygo interferometer (Forman 1979), shown in Fig. 1.23, and the Wyko interferometer, shown in Fig. 1.24.

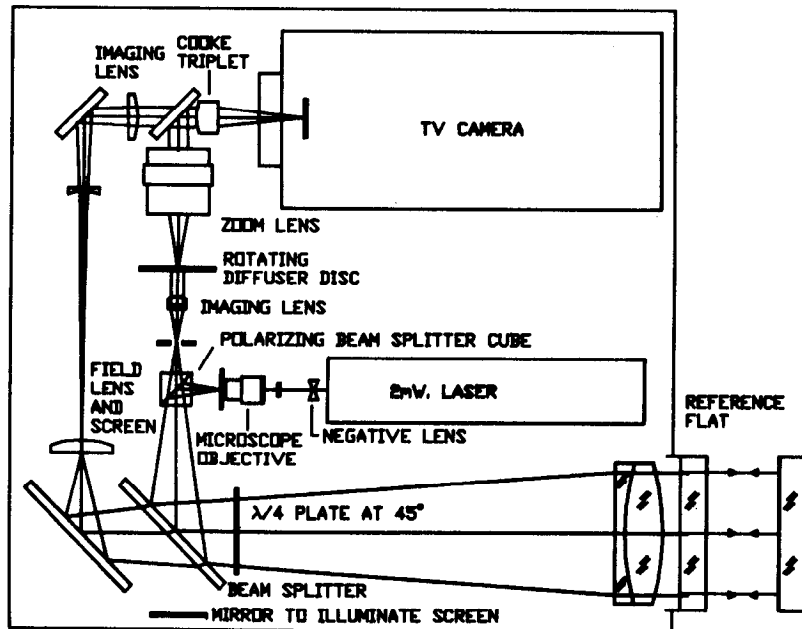


Figure 1.23. Fizeau interferometer manufactured by Zygo Corp. (Courtesy of Zygo, Corp.)

1.2. FIZEAU INTERFEROMETER

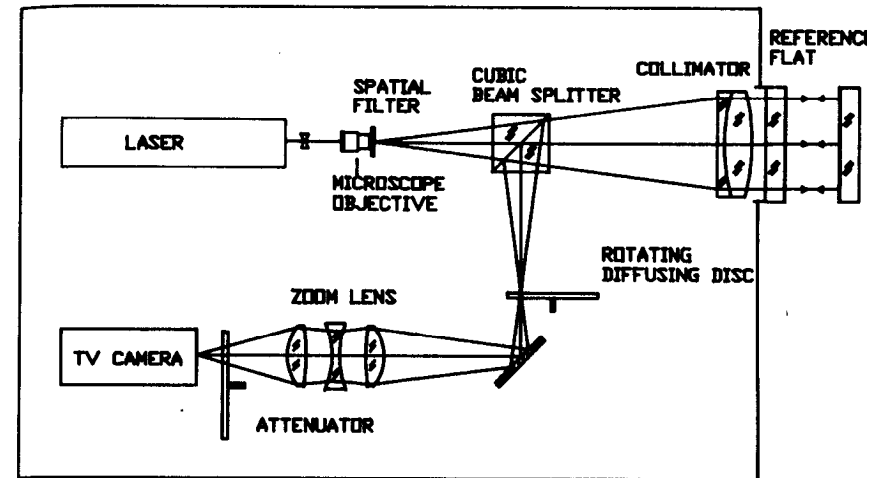


Figure 1.24. Fizeau interferometer manufactured by Wyko Corp. (Courtesy of Wyko, Corp.)

7.1.2 Twyman-Green Interferometer

The basic use of a Twyman-Green interferometer for measuring surface height variations was previously described. The Twyman-Green and Fizeau give the same interferograms for testing surface flatness; the main advantages of the Twyman-Green are more versatility and it is a non-contact test, so there is less chance of scratching the surface under test, while the main disadvantage is that more high-quality optical components are required.

7.1.3 Ritchey-Common Test

8.6. RITCHEY-COMMON TEST

According to Ritchey (1904), this test was suggested by a Mr. Common as a way of testing large optical flats (Shu 1983). For this purpose a good spherical mirror is used, with the flat acting also as a mirror, to obtain an apparatus similar to the one used for the knife-edge test. See Fig. 8.32.

Any small spherical concavity or convexity of the surface under test appears as an astigmatic aberration in the image of the illuminating point source. The

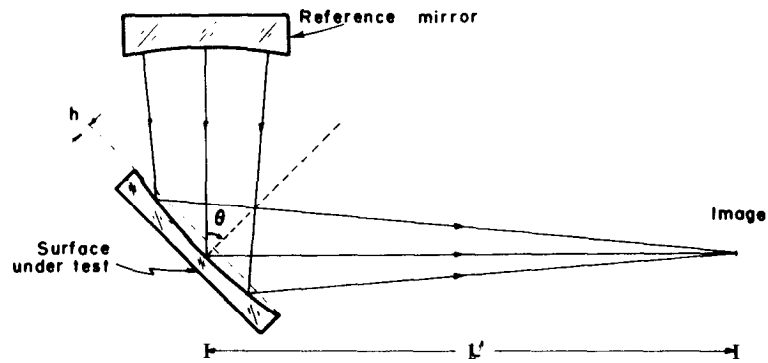


Figure 8.32. Geometry of the Ritchey-Common test.

two focal planes associated with the sagittal and tangential foci can be accurately found (by employing the knife-edge test as indicated in Section 8.1), and with this information the radius of curvature of the surface under test can be calculated. Of course, any localized deformation or deviation from flatness can also be observed.

The advantage of the Ritchey-Common test over other methods is that a reference flat is not needed as in the Newton or Fizeau interferometer. The autocollimation method requires a paraboloid as large as the largest dimension of the flat under test. On the other hand, the auxiliary mirror used in the Ritchey-Common test has a spherical shape, which is the easiest to make and test. An additional advantage is that the spherical mirror needs to be only as large as the minor diameter, if it is elliptical, like many diagonal mirrors used in telescopes or other instruments.

If we measure the astigmatism, we can obtain the magnitude of the concavity or convexity of the "flat" mirror, but it is assumed that this mirror is spherical, not toroidal, in shape. If the mirror is not circular but is elliptical, the possibility that it will develop a toroidal shape while being polished is very high. This toroidal shape introduces an additional astigmatism that complicates the analysis. Interested readers can consult the work of Tatian (1967), Silvemil(1973), and Shu (1983).

The mathematical description given here assumes that the mirror under test is not toroidal and follows the approach used by Couder (1932) and Strong (1938), that is, finding the curvature from the Coddington equations for astigmatism. In what follows it is assumed that the pinhole size source and the wire travel together, in the same plane. Hence, when evaluating the transversal ray aberrations, it is necessary to multiply the value obtained in this way by a factor of 0.5 to get the real value of the transverse my aberrations. However, since the aberrations of the wavefront arc duplicated in the Ritchey-Common test because of the double reflection on the optical flat under test, we can conve-

niently omit the double reflection factor of 2 and the factor 0.5 when calculating the value of the transversal ray aberrations.

Applying the well-known Coddington equations for astigmatism to a reflecting surface, we find that the sagittal focus of a converging beam incident on an optical reflecting surface is given (see Fig. 8.33) by

$$\frac{1}{s'} = \frac{1}{s} + \frac{2 \cos \theta}{r} \quad (8.88)$$

and the tangential focus by

$$\frac{\cos^2 \theta}{t'} = \frac{\cos^2 \theta}{t} + \frac{2 \cos \theta}{r} \quad (8.89)$$

where θ is the angle of incidence at the surface under test and r is the radius of curvature of the optical surface under test.

If we assume that the incident beam is free from astigmatism, that is, $s = t$, Eqs. (8.88) and (8.89) can be used to obtain

$$\frac{s' - t'}{s' t'} = \frac{2 \sin^2 \theta}{r \cos \theta} \quad (8.90)$$

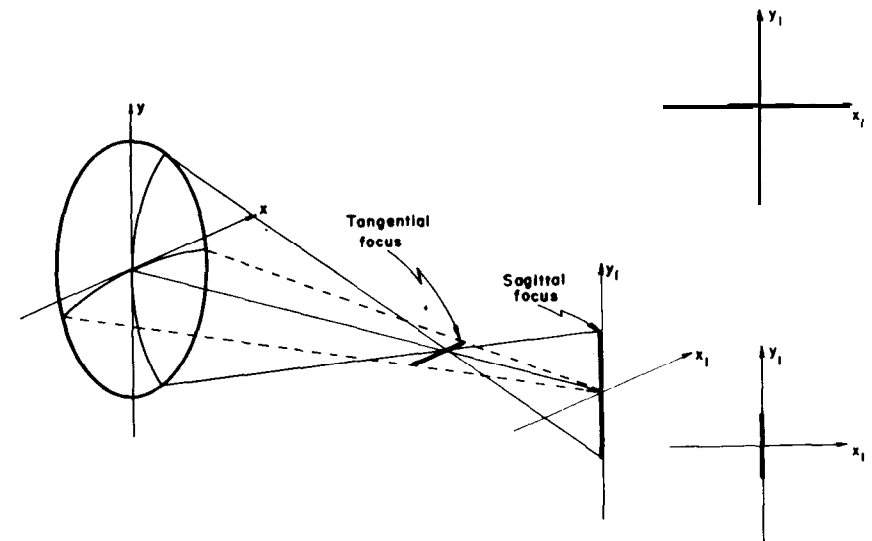


Figure 8.33. An astigmatic wavefront and its associated focal images. It is to be noted that the orientations of the images are changed when the setup in Fig. 8.32 is used. That is, the sagittal image is a horizontal line and the tangential image is a vertical one.

Now, by denoting $s' = L' + \delta L'$ and $t' = L'$, and substituting these values in Eq. (8.90), we have

$$r = 2L' \left(1 + \frac{L'}{\delta L'} \right) \frac{\sin^2 \theta}{\cos \theta}. \quad (8.91)$$

Since $|L' / \delta L'| > 1$, it follows from Eq. (8.91) that, when the sagittal focus is longer than the tangential focus ($\delta L' > 0$), the surface under test has a positive radius of curvature, that is, the surface is convex. On the other hand, when the sagittal focus is shorter than the tangential focus ($\delta L' < 0$), the surface has a negative radius of curvature and is concave. The sagitta h of a surface with a diameter D and a radius of curvature r can be approximated by

$$\delta L' \approx \frac{2L'^2}{r} \frac{\sin^2[\theta]}{\cos[\theta]} \quad h = \frac{D^2}{8r}. \quad (8.92)$$

Using Eq. (8.91) in (8.92) we have

$$h = \frac{D^2 \cos \theta}{16L' (1 + L' / \delta L') \sin^2 \theta}$$

For $L' \gg \delta L'$ ($|L' / \delta L'| \gg 1$), Eq. (8.93) reduces to

$$h = \frac{D^2 \delta L' \cos \theta}{16L'^2 \sin^2 \theta},$$

which gives the value for the sagitta of the optical surface under test for any angle of incidence θ . For the particular case of $\theta = 45^\circ$, the sagitta is given by

$$h = \frac{D^2 \delta L'}{11.3L'^2}. \quad (8.95)$$

Couder (1932 in Texereau 1957) has indicated that an optimum angle for testing optical flats is $\theta = 54^\circ 45'$. Of course, in practice it is more convenient to set $\theta = 60^\circ$. It is also common practice to use any eyepiece, instead of the knife edge, to determine visually the positions of the sagittal and tangential foci, by locating the positions of the patterns shown to the right of Fig. 8.33.

8.7 CONCLUSIONS

As mentioned in the introduction of this chapter, the examples examined demonstrate the versatility and usefulness of the Schlieren techniques and the related

phase modulation tests. Of course, the choice of any particular test depends on the circumstances.

To appreciate the sensitivity of the test, it is of interest to do a sample calculation. Let a flat have a 60-inch diameter, $\theta = 60^\circ$, and $L = 200$ inches. If $\delta L' = 0.01$ inch, the sag $h = 37.5$ microinch (approx 1.7λ), and $r = 10^6$ ft.

It is important to note that if the distance between the two line foci is measured, it is not necessary to measure the distance between the reference sphere and the flat, nor is it necessary to know the radius of curvature of the sphere. However, if only the difference in curvature of the tangential and sagittal fan is measured for a single focal position, it is necessary to know both the distance between the flat and the spherical mirror, and the radius of curvature of the spherical mirror. Hence, the test is generally performed as described.

Another important item is that if a null test is obtained, the mirror may not be a flat, it may be a hyperbola. To check to make sure that the mirror is flat, the mirror should be rotated 90° and the test repeated.

Although the Ritchey-Common test is great for measuring the radius of curvature of a nearly flat surface, it is difficult to measure accurately local irregularities. Neglecting higher order effects due to variation in surface angle, if α is the angle of incidence a ray makes with respect to the surface, and if the surface is tested in double pass, a local irregularity of height δ will introduce an OPD of

$$\text{OPD} = 4\delta \cos \alpha$$

Since α varies over the surface, it becomes difficult to accurately obtain d as a function of position on the mirror surface. Also, it should be noted that as the angle of incidence is increased, the sensitivity of the test to local irregularities decreases.

7.1.4 Naked Eye Test

Ref: Johnson, Optics and Optical Instruments, p. 196

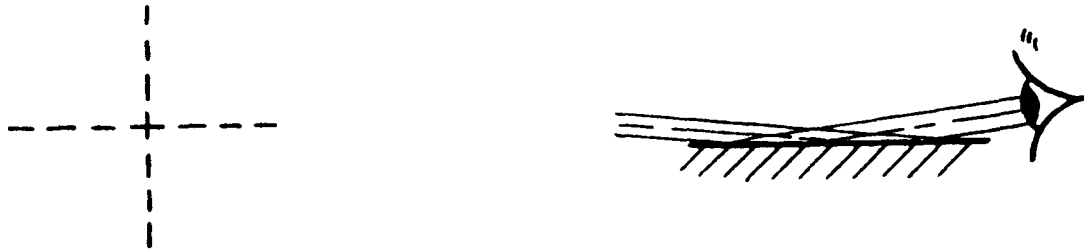


FIG. 222.
Naked Eye Test for Flatness of a Surface.

Naked Eye Test for Flatness of a Surface.

The test of a flat surface by oblique reflection is so sensitive that even the naked eye will detect quite a low degree of sphericity if nearly grazing incidence is employed. If a dotted cross, Fig. 222, is set up at a distance and an image of this is viewed in the surface so as to send light from the full length of the plate through the pupil of the eye, then any astigmatism resulting from the spherical form of the surface will cause the dots of either the vertical or horizontal line to merge together into a grey line. It may be estimated that the naked eye will thus detect a radius of curvature up to about ten thousand times the length of the surface being tested, provided that the surface measures at least several times the diameter of the pupil.

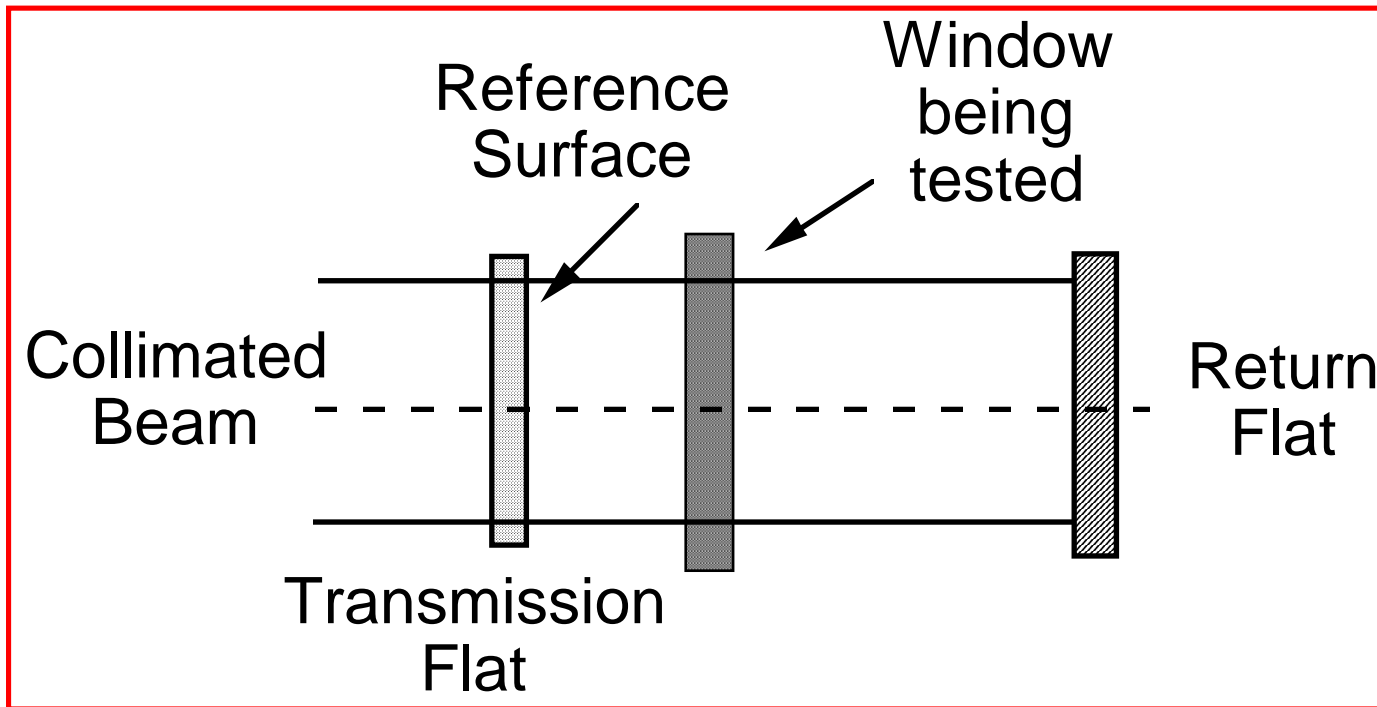
7.2 Windows

The most common instrument for testing windows is an interferometer. For measurement of window parallelism both interferometers and autocollimators are used.

7.2.1 Interferometers

Thickness variations can be measured using the setup shown in the next viewgraph.

Testing Windows in Transmission



δt = window thickness variations

$$\text{OPD measured} = 2 (n-1) \delta t$$

This same approach can be used to measure window surface parallelism (wedge). First the interferometer is adjusted so a single interference fringe covers the interference field. Next, the sample to be tested is placed in the cavity. If the sample has an appropriate amount of wedge, interference fringes will be observed. The OPD introduced for a window of diameter D, refractive index n, and wedge α , is given by

$$\text{OPD} = 2(n-1)\alpha D.$$

The fringe spacing, S, is then given by

$$S = \frac{\lambda}{2(n-1)\alpha}$$

If the sample is tested in a Mach-Zehnder interferometer a similar expression results, except there is no 2 in the denominator.

A second interferometric technique is to block off one mirror and replace the second mirror with the sample to be measured. Thus, the interference fringes result from the interference of the wavefronts reflected off the two surfaces of the sample. The fringe spacing is given by

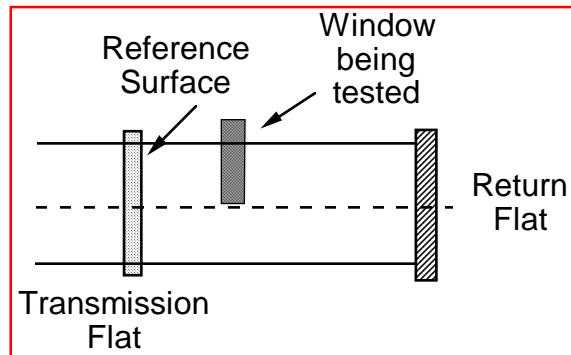
$$S = \frac{\lambda}{2n\alpha}$$

Table 1 gives fringe spacing S as a function of α for both double pass transmission and the reflection case.

Table 1. Fringe spacing as a function of wedge angle α for $n = 1.5$, $\lambda = 633$ nm					
α (sec)	S (mm) 1/S (1/mm)			S (mm) 1/S (1/mm)	
	Double Pass Transmission			Reflection	
1	126.6	0.008		42.20	0.024
5	25.32	0.039		8.44	0.118
10	12.66	0.079		4.22	0.237
30	4.22	0.237		1.41	0.711
60	2.11	0.474		0.70	1.422

The next viewgraph shows a convenient setup for measuring window wedge in a phase-shifting interferometer where it is not necessary to adjust the interferometer for a single fringe in the absence of a sample.

Measuring Window Wedge

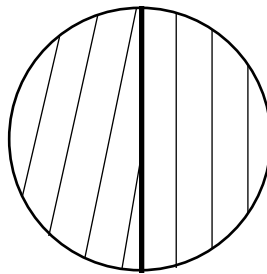


Tilt difference between two interferograms gives window wedge.

Optics 513 - James C. Wyant

Calculating Window Wedge

Tilt difference between two interferograms gives window wedge.

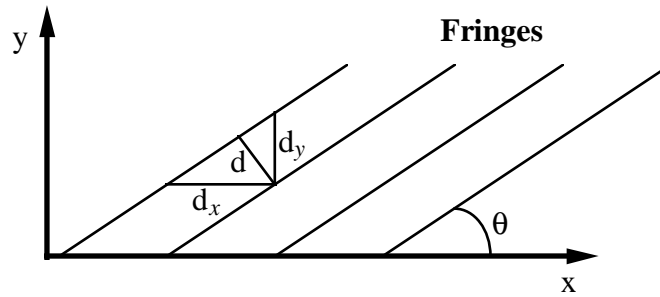


α = window wedge

$$\alpha = \frac{\text{tilt difference}}{2(n-1)}$$

Optics 513 - James C. Wyant

Calculation of Tilt



$d = \text{fringe spacing}$

$$d_x = d / \sin \theta$$

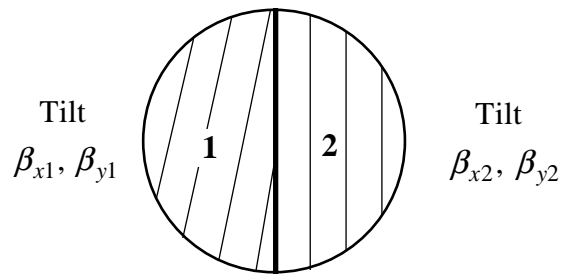
$$d_y = d / \cos \theta$$

$$\beta = \text{Tilt} = \frac{\lambda}{d}$$

$$\beta_x = \frac{\lambda}{d_x} \quad \beta_y = \frac{\lambda}{d_y}$$

Optics 513 - James C. Wyant

Calculation of Tilt Difference



$$\text{Tilt Difference} = \sqrt{(\beta_{x1} - \beta_{x2})^2 + (\beta_{y1} - \beta_{y2})^2}$$

Optics 513 - James C. Wyant

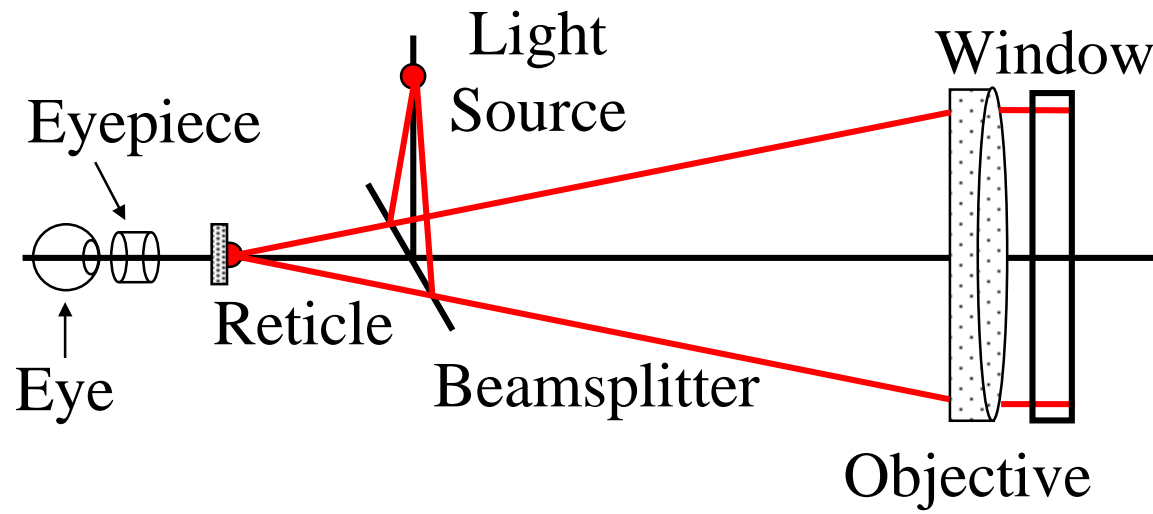
7.2.2 Autocollimator

The autocollimator is a telescope focused on infinity. A reticle is projected as a beam of parallel light from the objective. A flat front-surfaced mirror in the path of the beam will reflect back the image of the reticle, which is observed in the focal plane of the autocollimator. The position of the image depends upon the relative inclination of the mirror and the autocollimating telescope. If the relative inclination varies by an angle θ , the image actually moves through an angle 2θ . The instrument, whether it is read from a graduated reticle or microscope drum, yields a direct value and generally eliminates the necessity of doubling the reading.

The accuracy of an autocollimator for measuring angles is 1 sec of arc or less. Electronic autocollimators are made that have an accuracy of 0.01 sec of arc. Needless to say, for measurements having this accuracy, vibrations and air turbulence can cause much trouble.

To measure surface parallelism, one simply uses an autocollimator to observe the reflections off the two surfaces of a sample and measures the angular distance between the two reflections. If α is the wedge angle, the angular distance between the two reflected beams is $2n\alpha$. As described above, the calibration of the autocollimator *often* already accounts for the factor of 2.

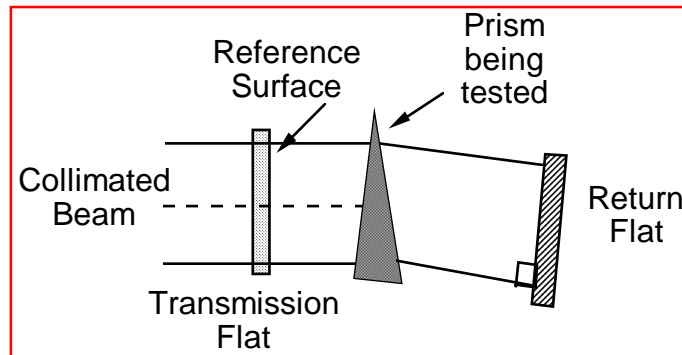
Autocollimator



7.3 Prisms

7.3.1 Interferometer

Testing Prisms in Transmission



δt = error in prism thickness

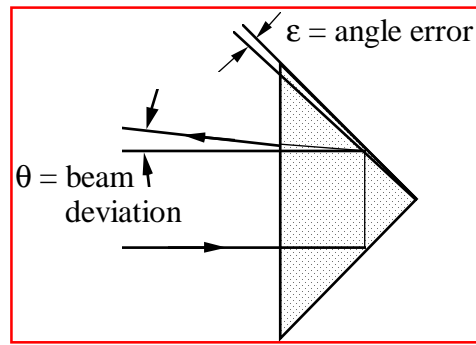
$$\text{OPD measured} = 2 (n-1) \delta t$$

Testing 90-Degree Prisms

Test Parameters

1. Surface accuracy of each face
2. Accuracy of angles
3. Material homogeneity
4. Transmitted wavefront accuracy

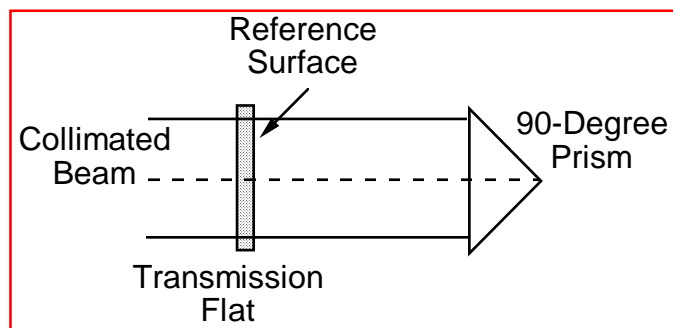
Angle Accuracy of 90-Degree Prisms



$$\epsilon = \frac{\theta}{2n}$$

Optics 513 - James C. Wyant

Testing 90-Degree Prisms (Single Pass)



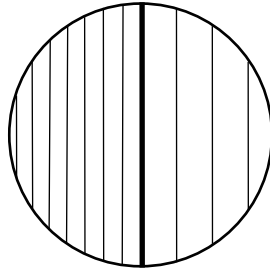
Tilt difference between two interferograms gives error in 90-degree angle.

Errors in collimated beam do not cancel.

Optics 513 - James C. Wyant

Calculating error in 90-Degree Prism (Single Pass)

Tilt difference
between two
interferograms
gives prism
angle error.

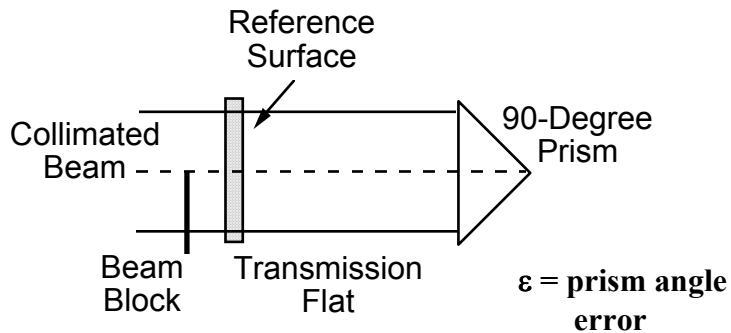


ϵ = prism angle
error

$$\epsilon = \frac{\text{tilt difference}}{4n}$$

Optics 513 - James C. Wyant

Testing 90-Degree Prisms (Double Pass)



$$\epsilon = \frac{x \text{ tilt in interferogram}}{4n}$$

Errors in collimated beam cancel.

Optics 513 - James C. Wyant

7.3.2 Goniometer

The most general instrument for measuring prism angles is the precision goniometer. A goniometer consists of a collimator, telescope, and a sample table, all arranged so they rotate about a common vertical axis. Divided circles on the underside of the instrument can accurately measure the angles of the collimator and telescope.

The goniometer is usually used in the autocollimating mode to measure the geometrical angles between the various faces of the prism under test. The addition of photoelectric systems to the goniometer has improved the acuity of setting by a factor of from 5 times to 10 times. An accuracy of such a photoelectric system can be better than 1 sec of arc.

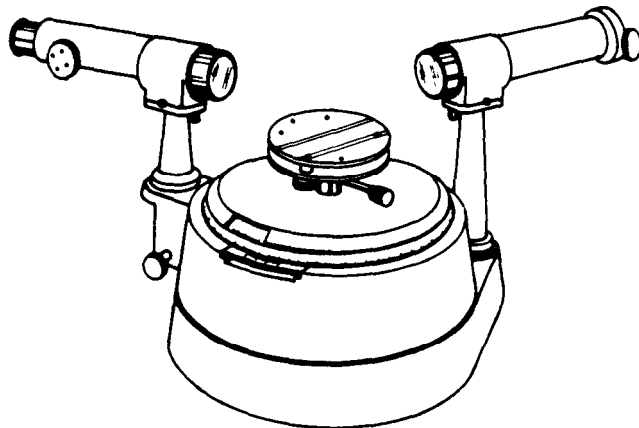


Figure 18.2. Goniometer.

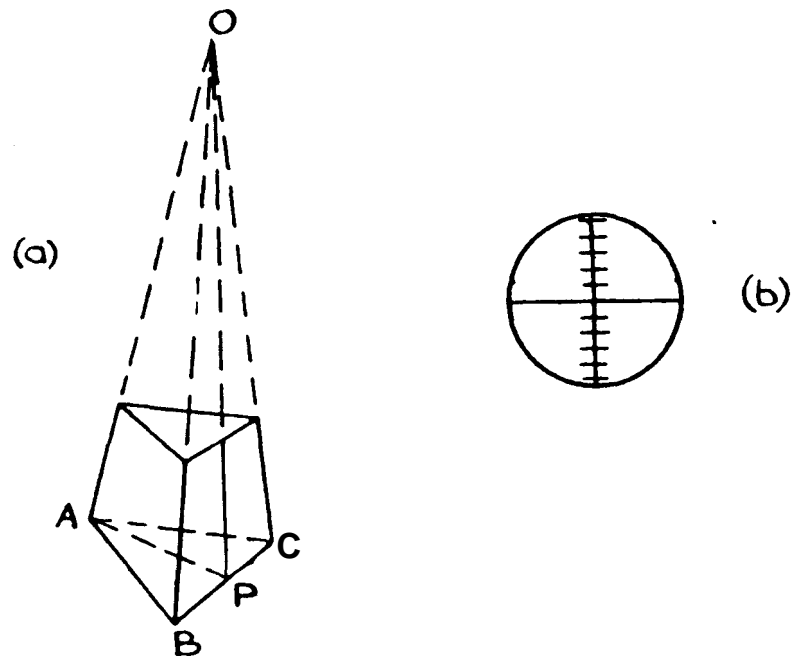


FIG. 223.
Pyramidal Error of Prisms.

Pyramidal Error.

In Fig. 223a, let the plane ABC be perpendicular to OA, and let AP be drawn perpendicular to BC, meeting it in P. If we join OP, then the angle AOP is a measure of the pyramidal error.

In order to measure this possible error, it is desirable to use a goniometer, such as that shown in Fig. 210, but with a graticule in the eyepiece of the form given in Fig. 223b. The telescope is directed towards faces AB and AC in turn, and the levelling screws of the prism table, together with the tilt of the telescope in a vertical plane, are adjusted so that the back reflected image of the horizontal graticule line falls on the real horizontal line in each case. When this adjustment has been effected, the edge AO of the prism must be perpendicular to the optical axis of the telescope.

If, now, the telescope is directed towards the face BC the displacement of the back-reflected horizontal line image can be measured on the vertical angular scale; this displacement will be equal to twice the angle AOP.

7.3.3 Autocollimator

The autocollimator described previously is used primarily for measuring prisms that are retroreflective, such as roof prisms and corner cube prisms. For example, if the angle of a roof prism is different from 90° by an angle ϵ , the two images will be seen in the eyepiece having a separation $2(2n\epsilon)$. The measurement is especially useful since its accuracy does not depend upon the angle of the entrance face, and thus no precise positioning of the prism is required.

See Fig. 213 and 214.

To determine the sign of the error put the prism on an optical flat. You should get the same error as before, except for the n factor. Tilt the prism as shown, and if the two images come together the exterior angle must be $> 90^\circ$, and if the images continue to separate the exterior angle must be $< 90^\circ$.

To determine the absolute values of the 45° angles the prism should be rested on the three balls as shown in Fig. 215. To prevent confusion from the other reflected images you may have to put some Vaseline on surfaces other than the hypotenuse. Having noted the reading of the reflected image on the eyepiece scale, the prism is now removed and placed on the three steel balls, such that the face AC now occupies that previously occupied by BC; the reading on the scale is again noted. The angular amount thus read off will represent twice the difference in angle between A and B. By observing the direction in which the image has moved, it can be shown which is the larger of the two angles, and since the value of the 90° angle is known, the true values of the 45° angles can be determined.

Sixty-degree angles can be measured as shown in Fig. 216. The prism is rested on the three balls and the auto-collimator arranged to receive light reflected from the face AB. The reflected image line is read on the eyepiece scale; the prism is then turned around so that the angle occupies the position previously held by A and the reading again taken on the scale. The difference in angle as given on the scale will be equal to twice the difference between angle A and angle C. Similarly, by placing angle B in the position of angle A, the difference of B from A may be obtained. Hence B and C can be expressed in terms of A in the equation $A + B + C = 180^\circ$. Having therefore determined the absolute value of angle A, those for B and C may also be obtained.

$$A + B + C = 180^\circ$$

$$2(A-C)=\alpha \quad 2(A-B)=\beta \quad C=(2A-\alpha)/2 \quad B=(2A-\beta)/2$$

$$A+A+A-\alpha/2-\beta/2 = 180^\circ$$

$$A=(180^\circ+\alpha/2+\beta/2)/3$$

Testing a corner cube with an autocollimator is more difficult since there are six beams returned, and the resulting image of the reticle will have too low a contrast to be useful. It is best if a mask is placed in front of the corner cube so only two beams are returned.

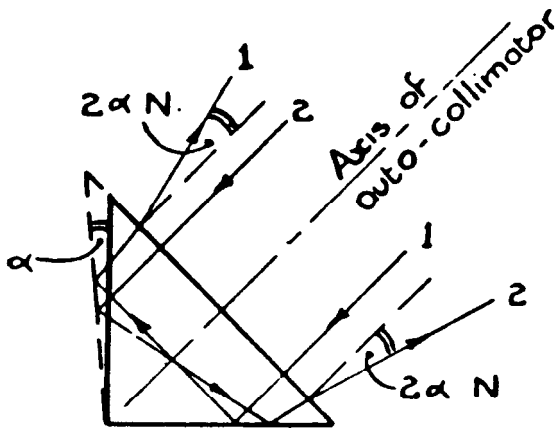


FIG. 213.

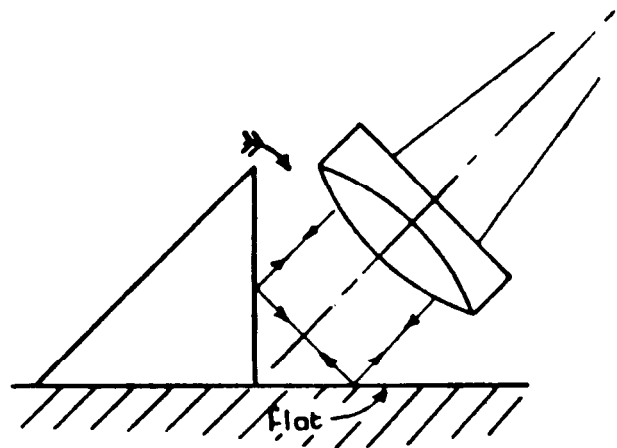


FIG. 214.

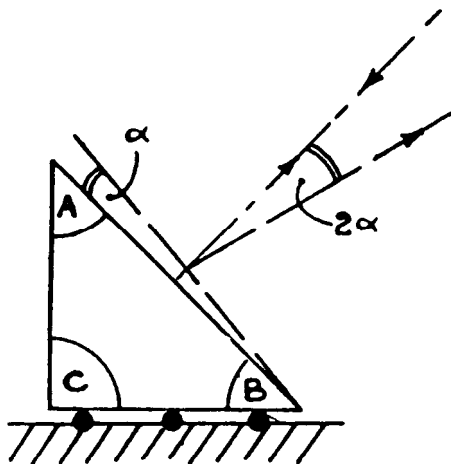


FIG. 215.

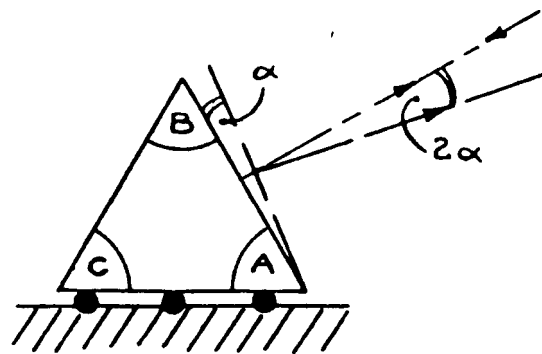


FIG. 216.

7.3.4 Naked Eye Tests

There are a couple of simple visual tests that can be used to obtain a rough check of $45^\circ - 90^\circ - 45^\circ$ prisms. The accuracy of the right angle can be determined by looking at the prism as shown in Figs. 218, 219, and 220. If the right angle is exactly equal to 90° , a perfectly round image of the iris of the eye is seen. If the angle is either slightly greater than or less than 90° , the image of the iris will become elliptical. The test can be improved by putting a card with lines on it and a circular hole in it in front of the eye.

$$\text{Error} = 4n\varepsilon \sim 6\varepsilon$$

Let $\varepsilon = 1$ minute, then error ~ 6 min

$$(60 \text{ cm}) (6 \text{ min}) \sim 1 \text{ mm}$$

Eye pupil ~ 4 mm, so 1 mm variation in roundness of image should be easily detectable.

The accuracy of the 45° angles on the prism can be determined by viewing a distant screen as shown in Fig. 221. If the angles are both 45° , no vertical image displacement will occur between light reflected directly from the hypotenuse of the prism and the light that passes through the prism. Horizontal displacement gives pyramidal error. The test will detect angle errors larger than a few minutes of arc. If ε is the difference between the two 45° angles, an error of $\sim (n-1)\varepsilon$ results. An accuracy of approximately 2 to 3 minutes is achievable.

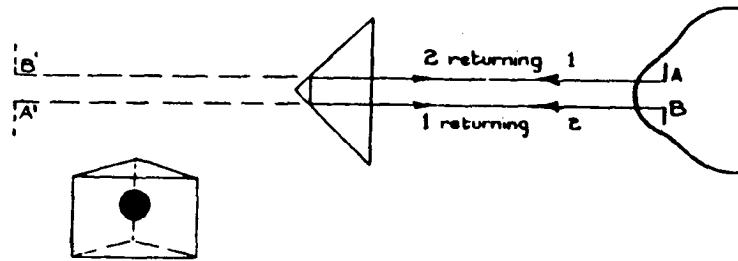


FIG. 218.

Naked Eye Tests on Prisms (90° Angle Correct).

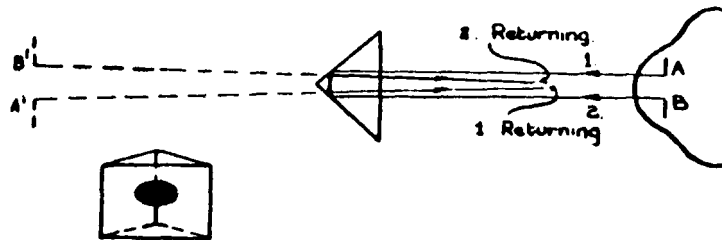


FIG. 219.

Right Angle less than 90° .

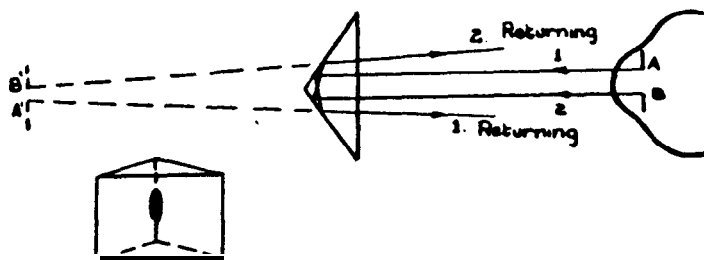


FIG. 220.

Right Angle greater than 90° .

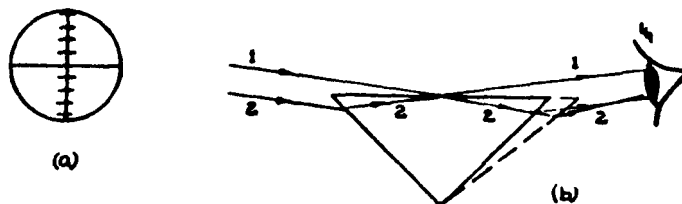


FIG. 221.

Test on Base Angles.

7.4 Corner Cubes

Let ε be the error in a 90° angle and the refractive index be n . As shown in Thomas and Wyant, for unit magnification this will cause the angular deviation, θ , between two output beams of

$$\theta = 4\sqrt{\frac{2}{3}}n\varepsilon \approx 3.266n\varepsilon$$

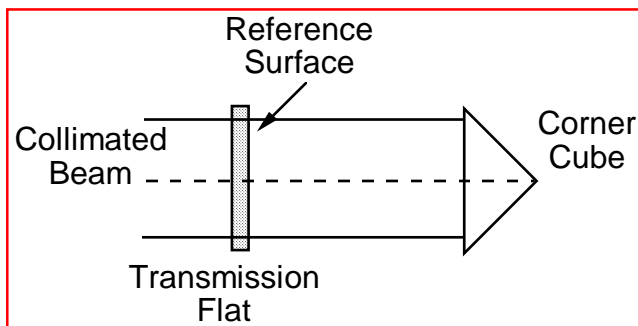
Testing Corner Cubes

Test Parameters

1. Surface accuracy of each face
2. Accuracy of angles
3. Material homogeneity
4. Transmitted wavefront accuracy

Optics 513 - James C. Wyant

Testing Corner Cubes (Single Pass)



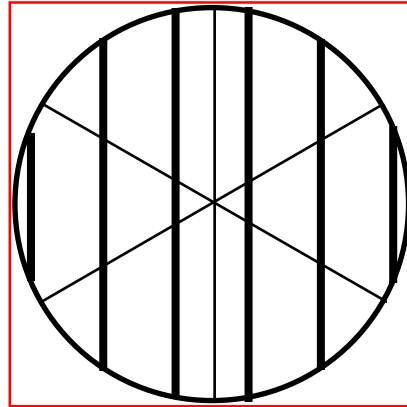
Errors in collimated beam do not cancel.

Optics 513 - James C. Wyant

Interferogram for Perfect Corner Cube (Single Pass)

6 interferograms obtained.

Straight fringes obtained for perfect corner cube.



Optics 513 - James C. Wyant

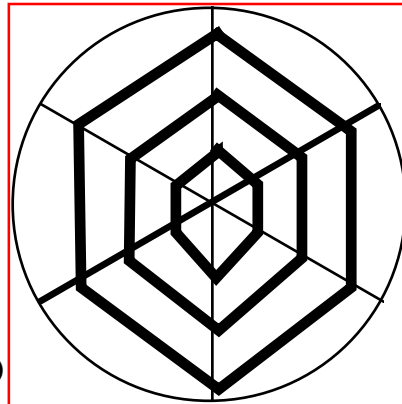
Analyzing Corner Cube Interferograms (Single Pass)

6 interferograms obtained.

Tilt difference between any 2 interferograms gives one angle error in corner cube.

n is refractive index of corner cube.

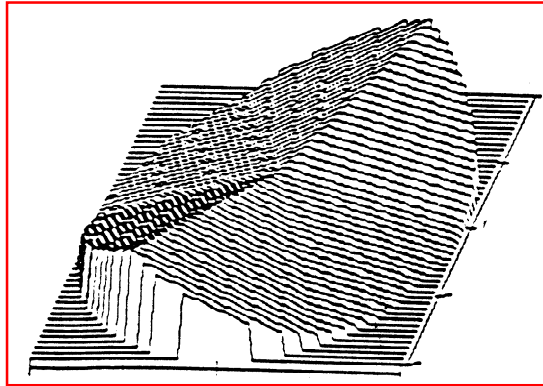
$$\text{Error} = \text{Tilt difference} / (3.266 n)$$



Optics 513 - James C. Wyant

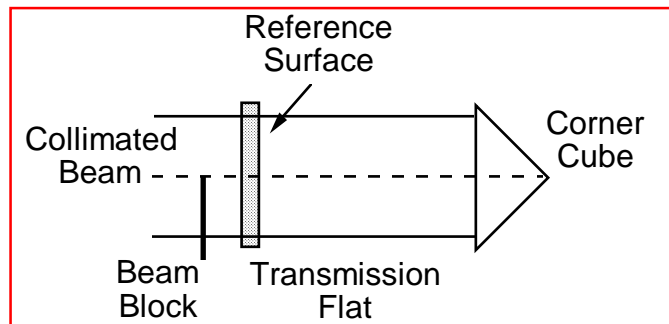
Corner Cube (Single Pass OPD)

RMS: 0.045 P-V: 0.191



Optics 513 - James C. Wyant

Testing Corner Cubes (Double Pass)



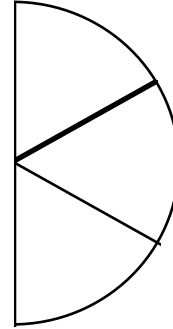
Errors in collimated beam cancel.

Optics 513 - James C. Wyant

Interferogram for Perfect Corner Cube (Double Pass)

3 interferograms obtained

One fringe covers the entire interferogram



Optics 513 - James C. Wyant

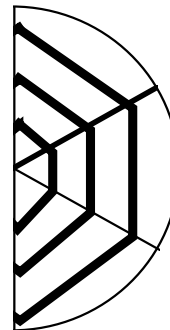
Analyzing Corner Cube Interferograms (Double Pass)

3 interferograms obtained.

Tilt of each interferogram gives one angle error in corner cube.

n is refractive index of corner cube.

$$\text{Error} = \text{Tilt}/(3.266 n)$$



Optics 513 - James C. Wyant

Determination of the dihedral angle errors of a corner cube from its Twyman-Green interferogram

David A. Thomas and J. C. Wyant

Optical Sciences Center, University of Arizona, Tucson, Arizona 85721

(Received 20 September 1976)

A technique is devised for calculating the magnitudes of the dihedral angle errors of a corner cube from a single Twyman-Green interferogram. Experimental examples are given in which the dihedral angles of two corner cubes are determined to within 2 arcsec by this procedure. These values are also shown to be in good agreement with independent goniometer measurements.

INTRODUCTION

Several authors have used the dot patterns produced by the reflection of a pencil of light from imperfect corner cubes to quantify their imperfections. Yoder¹ developed relationships that gave the deviation angles of the emerging beams with respect to the illuminating beam as a function of the three dihedral angle errors for the cube. He was able to favorably compare his calculated deviation angle values to the figures obtained directly from the dot patterns, but had to rely on independent measurements of the dihedral errors for the input values of his calculations. Joseph and Donahue² used the pattern data to compute the relative sign and magnitude of all three dihedral angle errors.

Corner cubes can also be readily tested with a Twyman-Green interferometer. Such interferograms are, in fact, often supplied by manufacturers as evidence of the quality of their product. When a perfect cube is tested in this fashion, the prism aperture is covered by a single sinusoidal fringe pattern. Imperfect prisms with planar reflecting surfaces generally have six distinct sinusoidal fringe patterns over their apertures. The patterns are usually inclined at various angles with respect to one another, and each one generally has a different spatial frequency. This paper describes the use of such an interferogram to determine the magnitudes of the dihedral angle errors of a corner cube. The derivation follows Yoder's basic matrix algebra approach.

THEORETICAL DEVELOPMENT

When a corner cube is viewed along its nominal axis of symmetry, its aperture is seen to be divided into six

equal triangular segments. When the prism is illuminated with a plane wave, a component plane wave will emerge from each of these segments. It is the interference between these emerging beams and a common reference plane wave that gives the fringe patterns mentioned in the introduction. An incident ray must undergo a sequence of three reflections in passing through the prism, and each of the six possible reflection sequences is associated with one of the aperture segments. If the three prism faces are numbered in a counterclockwise sequence starting with the lower face, the aperture segments would be associated with the reflection sequences indicated in Fig. 1. It is important to note that these segments can be grouped in pairs such that each member of a pair ' has a common face for its final reflection. This fact suggests that each corner cube dihedral angle error can be isolated by comparing the fringe patterns in one of these three pairs of aperture segments.

Since the angular orientations and spatial frequencies of the fringe patterns being examined depend on the angular relationships between the interfering beams, the theoretical treatment must be vectorial in nature. The propagation vectors for the six beams that emerge from a corner cube when it is illuminated by a single plane wave can be obtained by successively applying the vector law of reflection to the three reflecting surfaces. This law is derived in one of the references³ and can be written

$$\mathbf{S}_1 = \mathbf{S}_0 - 2(\mathbf{S}_0 \cdot \mathbf{M}) \mathbf{M}, \quad (1)$$

where \mathbf{S}_0 is the unit propagation vector for the incident beam, \mathbf{S}_1 the unit propagation vector for the reflected beam, and \mathbf{M} the outward pointing unit normal to the

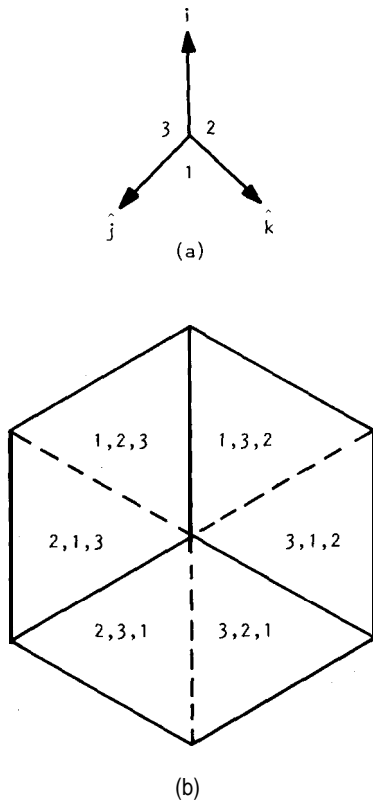


FIG. 1. Corner cube reflections. (a) Coordinate system and numbering sequence for reflecting surfaces. (b) Prism aperture with associated reflection sequences.

reflecting surface. This vector equation may be rewritten in matrix form as

$$\begin{bmatrix} S_{1x} \\ S_{1y} \\ S_{1z} \end{bmatrix} = \begin{bmatrix} (1 - 2M_x^2) & -2M_xM_y & -2M_xM_z \\ -2M_xM_y & (1 - 2M_y^2) & -2M_yM_z \\ -2M_xM_z & -2M_yM_z & (1 - 2M_z^2) \end{bmatrix} \begin{bmatrix} S_{0x} \\ S_{0y} \\ S_{0z} \end{bmatrix} \quad (2)$$

In this form the equation shows that a three-by-three reflection matrix $[R]$ characteristic of the reflector can be used to map an incident ray into its conjugate reflected ray. For a series of three reflections, we have

$$[S]_{ijk}^1 = [R]_{jk} [R]_j [R]_i [S_0], \quad (3)$$

or

$$[S]_{ijk}^1 = [R]_{ijk} [S_0] \quad (4)$$

where $i, j, k = 1, 2, 3$ and $i \neq j \neq k$. Once the direction cosines of the unit normals to the three reflecting surfaces of a corner cube are known, system reflection matrices can be calculated for each of the six possible sequences of reflections that can be used to map the illuminating ray into each of the final exiting rays.

If we assume that the dihedral angles are only slightly in error, we can write them as $(\pi/2 + \epsilon)$. If we also designate the angle between a pair of surface normals by θ , then $\cos \theta = \sin \epsilon$, and we can now write the various values of θ as

$$\cos \theta_{12} = M_{1x}M_{2x} + M_{1y}M_{2y} + M_{1z}M_{2z} = \sin \epsilon_{12},$$

$$\cos \theta_{13} = M_{1x}M_{3x} + M_{1y}M_{3y} + M_{1z}M_{3z} = \sin \epsilon_{13}, \quad (5)$$

$$\cos \theta_{23} = M_{2x}M_{3x} + M_{2y}M_{3y} + M_{2z}M_{3z} = \sin \epsilon_{23}.$$

The prism must now be given a specific orientation with respect to the Cartesian coordinate axes in order to specify the components of the three surface normals. We assume for computational convenience and without loss of generality that M_1 coincides with \hat{i} and that the dihedral edge between surfaces 1 and 2 is parallel to \hat{k} . This scheme was originally introduced by Yoder and can be used in conjunction with the fact that the surface normals must have unit length to show that

$$M_{1x} = 1, \quad M_{2x} = \sin \epsilon_{12}, \quad M_{3x} = \sin \epsilon_{13},$$

$$M_{1y} = 0, \quad M_{2y} = \cos \epsilon_{12}, \quad M_{3y} = (\sin \epsilon_{23} - \sin \epsilon_{12} \sin \epsilon_{13}) / \cos \epsilon_{12},$$

$$M_{1z} = 0, \quad M_{2z} = 0, \quad M_{3z} = (1 - M_{3x}^2 - M_{3y}^2)^{1/2}. \quad (6)$$

To a first-order small angle approximation, $\cos \epsilon = 1$ and $\sin \epsilon = \epsilon$, and the surface normal coordinates reduce to

$$M_{1x} = 1, \quad M_{2x} = \epsilon_{12}, \quad M_{3x} = \epsilon_{13},$$

$$M_{1y} = 0, \quad M_{2y} = 1, \quad M_{3y} = \epsilon_{23}, \quad (7)$$

$$M_{1z} = 0, \quad M_{2z} = 0, \quad M_{3z} = 1.$$

By substituting these coordinates into the reflection matrix given in Eq. (2), the reflection matrices obtained for the three corner cube faces are

$$[R]_1 = \begin{bmatrix} -1 & 0 & 0 \\ 0 & 1 & 0 \\ 0 & 0 & 1 \end{bmatrix},$$

$$[R]_2 = \begin{bmatrix} 1 & -2\epsilon_{12} & 0 \\ -2\epsilon_{12} & -1 & 0 \\ 0 & 0 & 1 \end{bmatrix}, \quad (8)$$

$$[R]_3 = \begin{bmatrix} 1 & 0 & -2\epsilon_{13} \\ 0 & 1 & -2\epsilon_{23} \\ -2\epsilon_{13} & -2\epsilon_{23} & -1 \end{bmatrix}.$$

The system reflection matrix for each of the six possible sequences of corner cube reflections can now be obtained by multiplying the component matrices given in Eq. (8) in the appropriate order. For example,

$$[R]_{123} = \begin{bmatrix} 1 & 0 & -2\epsilon_{13} \\ 0 & 1 & -2\epsilon_{23} \\ -2\epsilon_{13} & -2\epsilon_{23} & -1 \end{bmatrix}$$

$$\times \begin{bmatrix} 1 & -2\epsilon_{12} & 0 \\ -2\epsilon_{12} & -1 & 0 \\ 0 & 0 & 1 \end{bmatrix} \begin{bmatrix} -1 & 0 & 0 \\ 0 & 1 & 0 \\ 0 & 0 & 1 \end{bmatrix}, \quad (9)$$

or

$$[R]_{123} = \begin{bmatrix} -1 & -2\epsilon_{12} & -2\epsilon_{13} \\ 2\epsilon_{12} & -1 & -2\epsilon_{23} \\ 2\epsilon_{13} & 2\epsilon_{23} & -1 \end{bmatrix} . \quad (10)$$

Similarly,

$$[R]_{231} = \begin{bmatrix} -1 & 2\epsilon_{12} & 2\epsilon_{13} \\ -2\epsilon_{12} & -1 & -2\epsilon_{23} \\ -2\epsilon_{13} & 2\epsilon_{23} & -1 \end{bmatrix} \text{ and} \quad (11)$$

$$[R]_{312} = \begin{bmatrix} -1 & -2\epsilon_{12} & 2\epsilon_{13} \\ 2\epsilon_{12} & -1 & 2\epsilon_{23} \\ -2\epsilon_{13} & -2\epsilon_{23} & -1 \end{bmatrix} .$$

The remaining reflection sequences are the reverse of the three sequences indicated in Eqs. (10) and (11). Their system reflection matrices may be obtained from the corresponding forward sequence matrices above by reversing the signs on the matrix elements in the upper right and lower left quadrants while leaving the main diagonal elements unchanged.

Once an illuminating beam $[S_0]$ is specified, we can now find the reflected beam vectors $[S]_{ijk}$ for the corner cube by substituting each of our six system reflection matrices into Eq. (4). The prism is typically illuminated along its nominal axis of symmetry so that the aperture segments will have the same apparent size in the resulting interferogram. The $[S_0]$ direction cosines in this case are all equal to $\sqrt{3}/3$, and the correspond-

ing $[S]_{ijk}$ components are

$$\begin{aligned} S'_{x_{123}} &= -\sqrt{3}/3(1 + 2\epsilon_{12} + 2\epsilon_{13}), \\ S'_{x_{213}} &= -\sqrt{3}/3(1 + 2\epsilon_{13} - 2\epsilon_{12}), \\ S'_{y_{123}} &= -\sqrt{3}/3(1 + 2\epsilon_{23} - 2\epsilon_{12}), \\ S'_{y_{213}} &= -\sqrt{3}/3(1 + 2\epsilon_{12} + 2\epsilon_{23}), \\ S'_{z_{123}} &= -\sqrt{3}/3(1 - 2\epsilon_{13} - 2\epsilon_{23}), \\ S'_{z_{213}} &= -\sqrt{3}/3(1 - 2\epsilon_{13} - 2\epsilon_{23}), \end{aligned} \quad (12)$$

and so on.

The six beams that emerge from the corner cube are interfered with a common reference beam to obtain a Twyman-Green interferogram. In order for the fringe patterns to be visually resolvable, their spatial frequencies must be low and the reference beam must in turn be nearly, but not exactly, coincident with the illuminating beam. This will guarantee that a small number of fringes will appear across the prism aperture even in the event that the prism is perfect. We can represent the direction cosines of such a reference vector $[0]$ as $[-(1/\sqrt{3}) + \delta_1, -(1/\sqrt{3}) + \delta_2, -(1/\sqrt{3}) + \delta_3]$. To first order, both the reference beam vector just mentioned and the emergent beam vectors, such as those given in Eq. (12), are of unit length. Hence the cross product between reference beam and emergent beam not only points in the direction that the fringes resulting from the interference of these two beams would have, but also has a magnitude equal to the sine of the angle between the two vectors. This magnitude is, of course, also equal to the wavelength of light times the spatial frequency of the fringes.

Using the two rays given in Eq. (12) we can show that

$$\begin{aligned} [S]_{123} \times [0] &= \hat{i} [1/3(4\epsilon_{23} - 2\epsilon_{12} + 2\epsilon_{13}) - 1/\sqrt{3}(1 + 2\epsilon_{23} - 2\epsilon_{12})\delta_3 + 1/\sqrt{3}(1 - 2\epsilon_{13} - 2\epsilon_{23})\delta_2] \\ &+ \hat{j} [1/3(-2\epsilon_{23} - 2\epsilon_{12} - 4\epsilon_{13}) - 1/\sqrt{3}(1 - 2\epsilon_{13} - 2\epsilon_{23})\delta_1 + 1/\sqrt{3}(1 + 2\epsilon_{12} + 2\epsilon_{13})\delta_3] \\ &+ \hat{k} [1/3(-2\epsilon_{23} + 4\epsilon_{12} + 2\epsilon_{13}) - 1/\sqrt{3}(1 + 2\epsilon_{12} + 2\epsilon_{13})\delta_2 + 1/\sqrt{3}(1 + 2\epsilon_{23} - 2\epsilon_{12})\delta_1] \end{aligned} \quad (13)$$

and

$$\begin{aligned} [S]_{213} \times [0] &= \hat{i} [1/3(4\epsilon_{23} + 2\epsilon_{12} + 2\epsilon_{13}) - 1/\sqrt{3}(1 + 2\epsilon_{23} + 2\epsilon_{12})\delta_3 + 1/\sqrt{3}(1 - 2\epsilon_{13} - 2\epsilon_{23})\delta_2] \\ &+ \hat{j} [1/3(-2\epsilon_{23} + 2\epsilon_{12} - 4\epsilon_{13}) - 1/\sqrt{3}(1 - 2\epsilon_{13} - 2\epsilon_{23})\delta_1 + 1/\sqrt{3}(1 - 2\epsilon_{12} + 2\epsilon_{13})\delta_3] \\ &+ \hat{k} [1/3(-2\epsilon_{23} - 4\epsilon_{12} + 2\epsilon_{13}) - 1/\sqrt{3}(1 - 2\epsilon_{12} + 2\epsilon_{13})\delta_2 + 1/\sqrt{3}(1 + 2\epsilon_{23} + 2\epsilon_{12})\delta_1]. \end{aligned} \quad (14)$$

These two fringe vectors, though complicated in form, differ only in the sign of their ϵ_{12} contributions. Subtracting Eq. (13) from (14) yields the difference vector

$$\begin{aligned} [S]_{213} \times [0] - [S]_{123} \times [0] &= (4/\sqrt{3})\epsilon_{12} [(1/\sqrt{3} - \delta_3)\hat{i} \\ &+ (1/\sqrt{3} - \delta_3)\hat{j} + (-2/\sqrt{3} + \delta_1 + \delta_2)\hat{k}]. \end{aligned} \quad (15)$$

If the quadratic factors in δ are neglected, the length of this resultant is given by

$$I_{\text{resultant}} = (4/\sqrt{3})\epsilon_{12} [2 - 4/\sqrt{3}(\delta_1 + \delta_2 + \delta_3)]^{1/2} . \quad (16)$$

By looking at the interference between the reference beam $[0]$ and the beam $[1]$ that would be reflected by a

perfect corner cube, we can evaluate the magnitude of the above $(\delta_1 + \delta_2 + \delta_3)$ factor

$$[1] \cdot [0] = 1 - 1/\sqrt{3}(\delta_1 + \delta_2 + \delta_3) = \cos\theta \approx 1 - \theta^2/2, \quad (17)$$

where θ = the angle between the two beams. The approximation given in the final step should be a good one since θ must be small for reasons given earlier. Equation (17) may be rearranged to get

$$\theta^2 = 2/\sqrt{3}(\delta_1 + \delta_2 + \delta_3) \quad (18)$$

or

$$(\delta_1 + \delta_2 + \delta_3) = \sqrt{3}/2 (\lambda F)^2 , \quad (19)$$

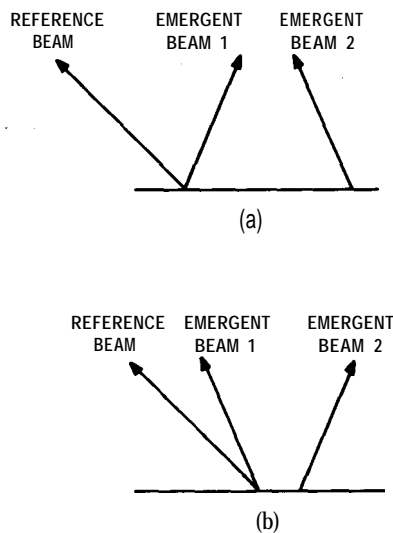


FIG. 2. Relative reference and emergent beam orientations that result in parallel fringe vectors. (a) Converging emergent beams. (b) Diverging emergent beams.

where F = the spatial frequency of the fringes that would be observed with a perfect corner cube. It should be noted that the fringe patterns associated with imperfect cubes will have spatial frequencies of the same order of magnitude as F since the various emergent beams make small angles with the illuminating beam in such cases provided the dihedral angle errors are small. Using Eq. (18) we can rewrite Eq. (16)

$$I_{\text{resultant}} = 4\sqrt{2/3} \epsilon_{12} [1 - (\lambda F)^2]^{1/2}. \quad (20)$$

For visible wavelengths and fringe spacings on the order of 1 mm or larger, $(\lambda F)^2$ is very small ($\sim 10^{-7}$) in comparison to unity, and we can say that, to a good approximation,

$$I_{\text{resultant}} = 4\sqrt{2/3} \epsilon_{12} \quad (21)$$

regardless of the particular reference beam used. If the above procedure is applied to $[S]_{231}'$ and $[S]_{321}'$ a difference vector magnitude of $4\sqrt{2/3} \epsilon_{23}$ is obtained while applying it to $[S]_{132}'$ and $[S]_{312}'$ yields a length of $4\sqrt{2/3} \epsilon_{13}$ for the difference vector.

It is of interest to note that the above three pairs of emergent beams correspond to the three pairs of prism aperture segments mentioned at the beginning of this section. The theory predicts that the magnitude of the dihedral angle error ϵ_{12} can be found by constructing vectors parallel to the fringes covering the aperture segments labeled "123" and "213" in Fig. 1 with lengths equal to the spatial frequencies of those fringes and then finding the length of the vector formed by subtracting one of these fringe vectors from the other. It also predicts that the magnitudes of ϵ_{13} and ϵ_{23} can be isolated using a similar analysis of the "132," "312" and "231," "321" pairs of fringe patterns, respectively.

The fringes that are recorded in a Twyman-Green interferogram are the projections of the actual fringes onto a plane that is nearly normal to the beam used to illuminate the corner cube. If the results obtained by the technique just described are to be accurate, we

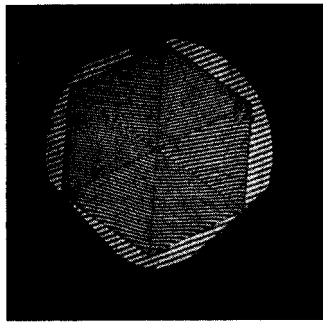
must be sure that the actual fringe vectors always lie sufficiently close to the interferogram plane to neglect their deviation from that plane. We know that if the beams reflected from the corner cube were interfered with a reference beam parallel to the beam used to illuminate the prism, the resulting fringes would all lie in the interferogram plane. We have shown that, for the reference beams that we expect to use, the angle between the reference and illuminating beams is equal to the product of the wavelength and fringe frequency, and that this product is on the order of 10^3 to 10^4 in magnitude. Thus for every case in which the assumptions we have already made concerning spatial frequencies of fringes are valid, the actual fringes should lie in planes that are sufficiently close to the interferogram plane for our above computational procedure to apply with good accuracy.

There is, of course, a problem involved in implementing this procedure experimentally. It is not obvious from examination of Twyman-Green interferograms what the directions of the associated fringe vectors should be. We can insure that the members of the above three pairs of fringe vectors both point in the same general direction for each pair by adjusting the reference beam prior to recording the interferogram so that it has an angular orientation outside that of the corresponding emergent beam vectors of each pair. Examples of this arrangement for vectors lying in one plane are illustrated in Fig. 2. Since the sense of rotation from the reference beam to each of the emergent beams in both of the cases shown in the figure is clockwise, the right-hand rule for determining the orientation of the cross product between two vectors predicts that the reference beam - emergent beam fringe vectors would all point into the plane of the paper in these examples. The above mentioned adjustment of the corner cube reference beam can normally be achieved in practice by selecting a reference mirror orientation that results in a large number of fringes over all the prism aperture segments. If the dihedral angle errors are all small, the emergent beams will make small angles with respect to one another so that reference beam orientations intermediate to any of the pairs of reflected beams being used to isolate these errors would result in low spatial frequency fringes over the corresponding pair of aperture segments. If the above precautions are taken in setting up a corner cube interferogram, the angles between the pairs of fringe vectors being used in the above subtraction process will always be given by the acute angles between the corresponding pairs of interferogram fringe patterns.

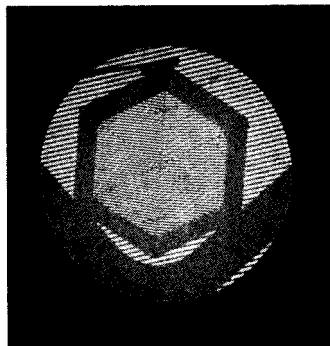
Finally, it should be noted that the ϵ_{ij} values calculated by the above technique should be divided by the refractive index to obtain the actual values when a glass prism is being tested interferometrically to compensate for refraction at the air-glass interface at the front of the corner cube.

EXPERIMENTAL VERIFICATION

Twyman-Green interferograms of a BK-7 glass corner cube and one consisting of front surface silvered



(a)



(b)

FIG. 3. Twyman-Green interferograms of two corner cubes. (a) BK-7 glass cube. (b) Front surface mirror cube.

mirrors are shown in Fig. 3. The fringe spacings and angular orientations of the fringe patterns in both interferograms were measured on a comparator. The acute angles between the pairs of fringe patterns needed to isolate the dihedral angle errors and the average spatial frequencies of all fringes were then calculated, and the results are given in Table I. The law of cosines was applied to the data in this table to find the lengths (in spatial frequency units) of the resultant vectors that were shown in the theory to be proportional to the dihedral angle errors. Finally, these errors (ϵ_{ij}) were computed from the difference vector lengths (L_{ij}) by means of the equation

$$\epsilon_{ij} = \lambda L_{ij} / 3.26mn \quad i=1, 2, \quad j=2, 3, \quad i \neq j. \quad (22)$$

The factor n stands for the prism index (1.514 for BK-7 or 1 for the mirror cube at $\lambda = 6563 \text{ \AA}$) and m stands for the ratio of the actual prism size to the interferogram

TABLE I. Comparator data for interferograms in Fig. 3.

Aperture segment	Glass cube		Mirror cube	
	Frequency (mm ⁻¹)	Relative angle (deg.)	Frequency (mm ⁻¹)	Relative angle (deg.)
213	1.92	3.72	1.99	0.55
123	1.61		1.87	
132	1.66	3.28	1.87	1.02
312	1.38		1.82	
321	1.63	18.54	1.92	5.25
231	1.62		1.91	

TABLE II. Dihedral angle error magnitudes for two corner cubes.

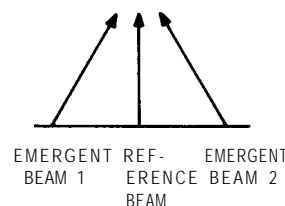
	Glass cube		Mirror cube	
	Computed value (arc sec)	Goniometer value (arc sec)	Computed value (arc sec)	Goniometer value (arc sec)
ϵ_{12}	7.59	-6.13	4.26	-3.35
ϵ_{13}	6.74	7.90	2.13	3.27
ϵ_{23}	12.03	-11.67	6.23	-5.25

size. This magnification factor is necessary because the fringe frequencies and the value of L , which is calculated in terms of them, depend on interferogram size and so must be corrected to the size of the prism. In our case, the values of m were 1.16 and 1.14 for the glass and mirror cubes, respectively. The computed errors are given in Table II for both corner cubes and are estimated to be accurate to within ± 1 arc sec. The primary cause for variation in the computed ϵ values about the average values given in the table was variation in the comparator line spacing measurements within a single fringe pattern. This variation was greatest for the BK-7 cube data and was due largely to fringe curvature caused by deviation in the prism reflecting surfaces from flatness.

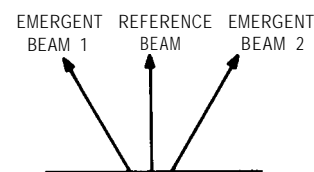
The dihedral angles in both corner cubes were also externally measured one at a time with a goniometer. These values are given in Table II and were also repeatable to within about ± 1 arc sec. It was, of course, possible to recover the signs as well as the magnitudes of the errors with the goniometer. Comparison of the corresponding error magnitudes obtained by the two methods shows agreement to within the accuracies of the measurements.

CONCLUSION

The procedure presented in this paper for recovering the magnitudes of the dihedral angle errors in a corner



(a)



(b)

FIG. 4. Relative reference and emergent beam orientations that result in parallel fringes of equal spatial frequency. (a) Converging emergent beams. (b) Diverging emergent beams.

cube from its Twyman-Green interferogram is convenient and apparently accurate. In the absence of additional information, it is, however, impossible to recover the signs of these errors from a single interferogram. A technique often used in interferometry to obtain information concerning the signs of errors is to adjust the tilt of the reference beam after the interferogram has been recorded and observe the resulting changes in the fringe patterns. For example, if the reference beam were oriented by appropriate adjustment of the interferometer reference mirror so as to give fringes of equal spatial frequency over one of the pairs of aperture segments being used to evaluate one of the dihedral angle errors, the corresponding beam orientations would be as shown in Fig. 4. A further clockwise rotation of the reference beam from the posi-

tion shown in the figure would result in an increase in the spatial frequency of the fringes resulting from the interference of the right-hand pair of beams if the emergent beams were converging ($\epsilon < 0$) and a decrease if they were diverging ($\epsilon > 0$). The same procedure applied to the other two pairs of fringe patterns would also give the signs of their associated dihedral angle errors.

¹P. R. Yoder, Jr., "Study of light deviation errors in triple mirrors and tetrahedral prisms," J. Opt. Soc. Am. 48, 496-499 (1958).

²Bernard W. Joseph and Robert J. Donohue, "Dot patterns from imperfect cube-corner reflectors," J. Opt. Soc. Am. 62, 727 (1972).

³Military Standardization Handbook 141, Defense Supply Agency, Washington, D. C., 13-1 through 13-9.

7.5 Testing of Diffraction Gratings

1) Ghosts

Periodic errors in spacing of grating grooves (result from errors extending over large areas of grating).

2) Satellites

False spectrum lines close to parent line (result from a small number of misplaced grooves in a localized part of the grating).

3) Scattered light

4) Efficiency

5) Direct wavefront testing using interferometer

For reflection gratings use Twyman-Green or Fizeau and for transmission gratings use Mach-Zehnder.

For perfect straight line grating

$$\frac{x}{\Delta x} = m; \quad \Delta x = \text{line spacing}; \quad m = \text{integer};$$

Errors in lines

$$\frac{x}{\Delta x} + \frac{\delta[x, y]}{\Delta x} = m$$

$\delta[x, y]$ = error in line position

Compare with interferogram or hologram

$e^{-i k x \sin[\theta]}$ represents amplitude of tilted plane wave

$e^{i k \Delta w[x, y]}$ represents wavefront having aberration $\Delta w[x, y]$

Irradiance of interference pattern given by

$$i = i_o (1 + \text{Cos}[k x \sin[\theta] + k \Delta w[x, y]])$$

For bright fringe

$$\frac{x \sin[\theta]}{\lambda} + \frac{\Delta w[x, y]}{\lambda} = m$$

Therefore, for grating the aberration in the first order in units of waves is

$$\frac{\delta[x, y]}{\Delta x}$$

N^{th} order will have N times as much aberration.

Interferometric Method of Measuring Plotter Distortion

J. C. Wyant, P. K. O'Neill, and A. J. MacGovern

The authors are with the Itek Corporation, Lexington, Massachusetts 02173.

Received 25 September 1973.

In this letter an interferometric method of measuring plotter distortion is described. A common method of measuring plotter distortion is to draw a known pattern, such as straight lines, and scan this pattern with a microdensitometer. This is a precise method of measuring distortion; however, it is a time consuming process; and it gives distortion only along the microdensitometer scan lines. The technique described below gives a contour map for the whole plot showing lines of constant distortion in a particular direction. By combining two contour maps for distortion in two orthogonal directions, the distortion in any arbitrary direction can be found. If the plotter distortion is repeatable and the plotter is computer controlled, once the distortion is known it can be eliminated as described by Fercher et al.^{1,2}

As will now be shown, if a plotter draws straight lines the plot can be thought of as a hologram produced by interfering two plane wavefronts. The plotter distortion produces the same effect on the plot as aberration in one of the plane wavefronts would produce on the hologram. If a plotter were to draw perfectly straight lines perpendicular to the x direction, the equation of the straight lines would be $(x / \Delta x) = M$, where Δx is the line spacing and M is an integer, 0, 1, 2, and so forth. Because of plotter distortion, the lines are never perfectly straight. Let the distortion in the x direction be $\delta x(x, y)$. Thus a point that should have the x coordinate x will have the x coordinate $x + \delta x(x, y)$. Therefore, the equation of the lines drawn by the plotter will be

$$\left[\frac{x}{\Delta x} \right] + \left\{ \frac{[\delta x(x, y)]}{\Delta x} \right\} = M. \quad (1)$$

Now consider the interference pattern (or hologram) formed by interfering two wavefronts. If a tilted plane wave, which can be represented as $e^{-ikx \sin \theta}$, where $k = 2\pi/\lambda$, and λ is the wavelength, and an aberrated plane wave represented as $\exp[ik\phi(x, y)]$ are interfered, a bright fringe is obtained every time the phase difference between the two interfering wavefronts is a multiple of 2π . That is, a fringe of order M is obtained when $kx \sin \theta + k\phi(x, y) = 2\pi M$. Dividing through by 2π yields

$$\frac{x \sin \theta}{\lambda} + \frac{\phi(x, y)}{\lambda} = M. \quad (2)$$

Equations (1) and (2) show that the plot of distorted straight lines can be thought of as a hologram made by interfering a tilted plane wave with an aberrated plane wave. A distortion δx equal to the average line spacing, Δx , corresponds to one wave of aberration. For example, if the plot lines are spaced 500μ , a distortion of 500μ corresponds to one wave of aberration. The above results can also be considered in terms of detour phase as previously described in the literature.^{3,4}

If the plot is recorded on photographic film and illuminated with a plane wave, several diffracted orders will be produced, just as would be produced by a diffraction grating or hologram. The first order will be an aberrated plane wave. The aberration function in units of waves is equal to $[\delta x(x, y) / \Delta x]$. As for a regular hologram, the second

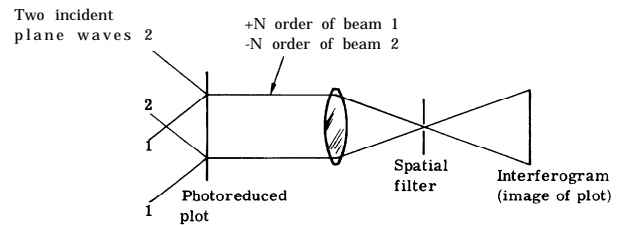


Fig. 1. Experimental setup for testing plot.

order will have twice as much aberration, the third order will have three times as much, etc.^{5,6,7} In general the N th diffracted order will have N times as much aberration as the first order. If the N th diffracted order is interfered with a plane wave, the resulting interferogram gives plotter distortion in the same manner as Twyman Green interferometers give wavefront aberration.

Figure 1 shows a convenient setup for testing a plot. Either the plot or a photo reduced version of the plot is illuminated with two plane wavefronts. The plot is reimaged as shown. A spatial filter (small aperture) is placed in the focal plane of the reimaging lens. The two plane wavefronts are incident upon the plot at the appropriate angle such that the $+N$ order as produced by beam 1 and the $-N$ order as produced by beam 2 pass thru the spatial filter. The number of fringes in the resulting interferogram is selected by adjusting the tilt of the two illuminating plane waves. If the lines drawn by the plotter are spaced a distance Δx , a fringe error in the interferogram corresponds to a distortion error of an integer multiple of $\Delta x / 2N$ in the plot. In general, any two diffracted orders can be interfered. It is convenient to pick $\pm N$, because, if the two incident plane waves have the same intensity, the two interfering wavefronts have the same intensity and good contrast interference fringes are obtained.

If the spatial filter shown in Fig. 1 is removed from the setup, the shape of the fringes in the interferogram is unchanged; however the contrast of the fringes is reduced. The interferogram obtained in this case is the moire, between the plot and the interference fringes formed by interfering plane waves 1 and 2.

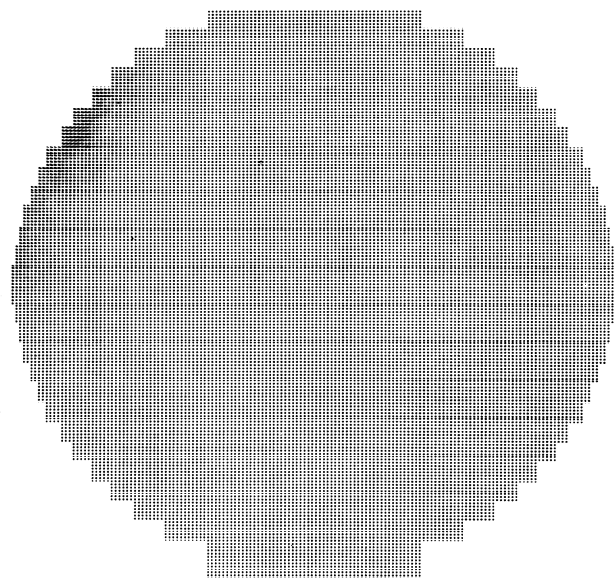
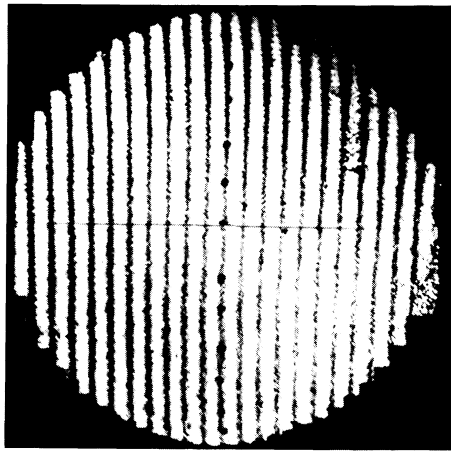


Fig. 2. Laser beam recorder plot.



Error in vertical lines

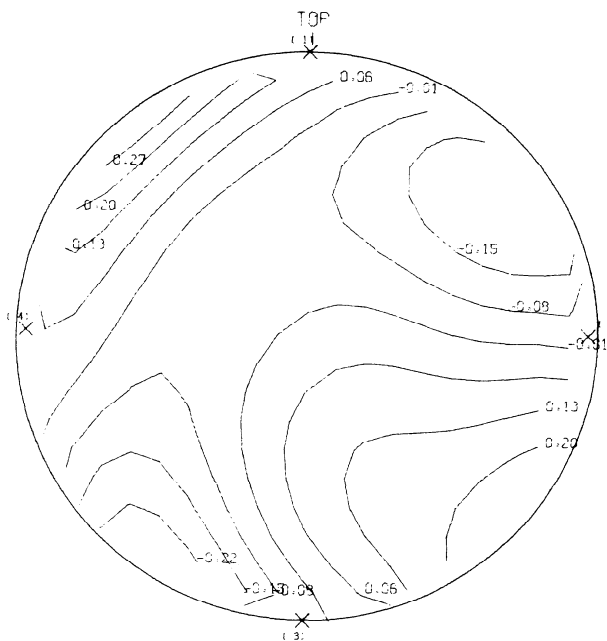


Fig. 3.
Distortion in x direction ($200 \mu\text{m}$ per wave).
Top: Error in vertical lines.
Bottom: error in vertical lines; peak-to-peak,
error = 0.69 wave = $138 \mu\text{m}$; RMS error = 0.13 wave = $26 \mu\text{m}$.

A good feature of the experimental setup shown in Fig. 1 is that if the plot is recorded on a photographic plate, the plate need not be extremely flat. If the two plane wavefronts are incident on the emulsion side of the plate, the two diffraction orders of interest will both see the same thickness variations. Thus, thickness variations in the plate will not affect the final interferogram.

It should be noted that if a photo reduced version of the plot is used in the test setup, instead of the actual plot, the combined distortion produced by both the plotter and

the photo reduction lens is being measured. This suggests using this technique for measuring lens distortion. If a straight line pattern having either essentially zero distortion, or at least known distortion, is photographed and the resulting transparency is placed in this setup, the distortion produced by the photo reduction lens can be obtained.

Figure 2 shows a plot drawn by a laser beam recorder. The diameter of the plot was approximately 20 cm and the spacing of the lines or dots was approximately $1200 \mu\text{m}$. The plot was photoreduced to a diameter of 2 cm . A two-dimensional dot pattern was drawn so distortion in both the horizontal and the vertical direction could be measured. The vertical lines give distortion in the horizontal direction, and the horizontal lines give distortion in the vertical direction.

Figure 3 shows results obtained measuring distortion in the x direction. The spatial filter shown in Fig. 1 was positioned to pass diffraction orders produced by the vertical lines. The tilt between the two incident plane waves was adjusted to produce the interference fringes shown. The fringe positions were measured and this data was put into a computer, which took out the tilt to obtain the contour map shown. The lines in the contour map are lines of constant distortion in the x direction. Since the lines on the original plot were spaced $1200 \mu\text{m}$ and $\pm 3\text{rd}$ diffraction orders were interfered, one fringe error in the interferogram corresponds to a distortion error of 1200 divided by 6 , or $200 \mu\text{m}$. By combining the results shown in Fig. 3 with similar results obtained for distortion in the y direction, the distortion in any desired direction can be found. If the plotter distortion is repeatable and the plotter is computer controlled, once the distortion is determined it can be eliminated.

Figure 4 shows a very interesting distortion error. The vertical lines drawn by the plotter in some cases were displaced horizontally about $80 \mu\text{m}$ from the correct position. Since the lines drawn by the plotter were spaced $1200 \mu\text{m}$, it was very difficult to see the $80\text{-}\mu\text{m}$ horizontal displacement in the plot. However, by using the technique described in this paper the error became very obvious, as shown in the figure. In summary, this letter describes an interferometric method of measuring plotter distortion in the same manner as Twyman Green interferograms give wavefront aberrations. Each interferogram gives dis-

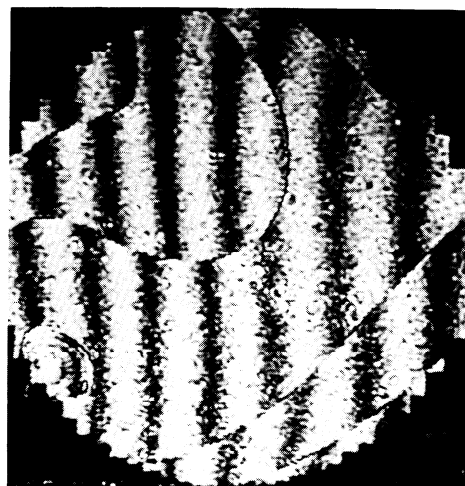


Fig. 4. Error in laser beam recorder lines ($200 \mu\text{m}$ per fringe).

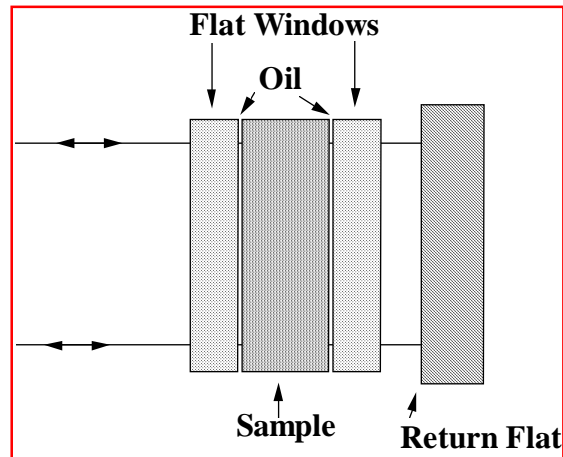
tortion in a particular direction. From two interferograms, giving distortion in two orthogonal directions, the distortion in any desired direction can be obtained. The technique can also be used to measure lens distortion.

The authors are indebted to the referee who pointed out Refs. 1 and 2.

References

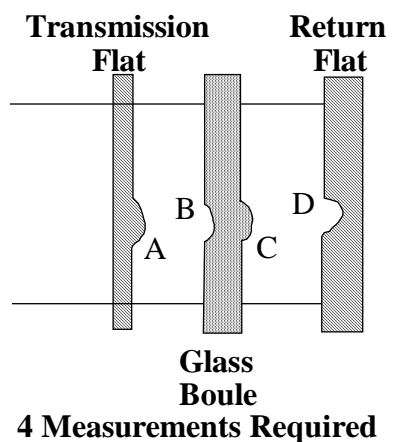
1. A. F. Fercher and M. Kriese, *Optik* 35, 168(1972).
2. A. F. Fercher, P. Skalicky, and J. Tomiser, *Opt. Laser Tech.* 5, 75(1973).
3. B. R. Brown and A. W. Lohmann, *Appl. Opt.* 5,967(1966).
4. A. W. Lohmann and D. P. Paris, *Appl. Opt.* 6,1739(1967).
5. O. Bryngdahl and A. W. Lohmann, *J. Opt. Soc. Am.* 58, 141(1968).
6. O. Bryngdahl, *J. Opt. Soc. Am.* 59,142(1969).
7. K. Matsumoto and M. Takashima, *J. Opt. Soc. Am.* 60, 30(1970).

Measuring Index Inhomogeneity (Classical Technique)



Optics 513 - James C. Wyant

Measuring Index Inhomogeneity Without Oil-On Plates



Surface Errors in Test Optics and Glass Boule Cancel.

Optics 513 - James C. Wyant

Measuring Index Inhomogeneity

1. Measure light reflected from front surface of boule.
 $OPD_1 = 2(B-A)$
2. Measure light through boule and reflected off second surface.
 $OPD_2 = 2(B-A) + 2n_o(C-B) + 2\delta$
3. Measure through boule and reflected off return mirror.
 $OPD_3 = 2(B-A) + 2n_o(C-B) + 2(D-C) + 2\delta$
4. Remove boule and measure cavity.
 $OPD_4 = 2(D-A)$

$$\delta = [n_o(OPD_3 - OPD_4) - (n_o - 1)(OPD_2 - OPD_1)] / 2$$
$$= (n - n_o)T$$

Optics 513 - James C. Wyant

Index Inhomogeneity Test Results

RMS: 0.168 wv P-V: 0.711 wv wv: 632.8nm



Optics 513 - James C. Wyant

Measurement of the inhomogeneity of a window

Chiayu Ai
WYKO Corporation
2650 E. Elvira Road
Tucson, Arizona 85706

James C. Wyant, FELLOW SPIE
WYKO Corporation
2650 E. Elvira Road
Tucson, Arizona 85706
and
Optical Sciences Center
University of Arizona
Tucson, Arizona 85721

Abstract. We describe three methods to measure the inhomogeneity of a window material. The first method immerses the window in a liquid between two planes. However, this method is inconvenient for some applications. The second method measures the optical figure of the front surface and then measures the return wavefront that transmits through the window and reflects from the rear surface of the window. The advantage of this method is that it can remove the contributions of both the surface figures and the return flat plus the system error of the interferometer. The disadvantage is that a small wedge must be fabricated between the two surfaces to eliminate spurious interference. The third method derives the inhomogeneity of the window material by measuring the optical figure of the front surface of the window and then flipping the mirror to measure the back surface. The advantage of this method is that it is not necessary to have a wedge between the two surfaces. The disadvantage of the window-flipping method is that the contribution of system error can increase.

Subject terms: optical window inhomogeneity; optical testing; index of refraction.
Optical Engineering 30(9), 1399-1404 (September 1991).

CONTENTS

1. Introduction
2. Three measurement methods
 - 2.1. Liquid immersion method
 - 2.2. Transmission method
 - 2.3. Window-flipping method
3. Experiment
4. Discussion
5. Conclusion
6. Acknowledgments
7. References

1. INTRODUCTION

The deformation of a transmitted wavefront through a window is due to a combination of the inhomogeneity of the window material and the figures of both surfaces of the window. Several methods have been proposed to measure the inhomogeneity.¹⁻⁵ In theory, if both surfaces are much better than the amount of the homogeneity of interest, any deformation of the wavefront is due to the inhomogeneity of the window material.

Opticians, however, want to know the inhomogeneity of a window material before precision polishing is done. Adachi et al.⁷ immersed a fine ground optical material into a cavity filled with a liquid of the same refractive index as the window. They were able to eliminate the contribution of both surfaces and measure the inhomogeneity of the window. The disadvantage of this method is that the use of a liquid is inconvenient for some applications. However, if both surface figures of the window are known, it is possible to derive the inhomogeneity of the window material. With the aid of a digital interferometer, it is possible to measure the figures of the two surfaces and store this information for later use. By mathematically manipulating the

data, we can subtract the contribution of both surfaces from the transmitted wavefront.

Schwider et al.⁵ measured the contribution of the rear surface with the wavefront transmitted through the window and reflected by the rear surface. Thus, they were able to remove the contributions of both surfaces, the return flat, and the system error of the interferometer with four measurements. Since the transmitted wavefront is used, we call this the transmission method. One disadvantage of this method is that a wedge has to be fabricated between the two surfaces to eliminate the spurious reflection. On the other hand, it is a straightforward procedure to measure the rear surface of the window by flipping the window and then removing its contribution to the transmitted wavefront. We call this the window-flipping method. However, the contribution of the system error can increase with this method.

In the following sections we compare the mathematical derivations for the transmission method and the window-flipping method and show the experimental results of the three methods. We also discuss the error analysis in details.

2. THREE MEASUREMENT METHODS

2.1. Liquid immersion method

The liquid immersion method uses two optical flats to form a cavity filled with a liquid. A window is dipped into a liquid that has the same refractive index as the window material. The liquid must be stable to perturbations and be harmless. The transmitted wavefront through the cavity reflects off a flat, and the return wavefront is measured with a digital interferometer. The contribution of the cavity is removed by taking the difference of two measurements with and without the window in the cavity.

2.2. Transmission method

In this section, we summarize the procedure given by Schwider et al.⁵ An interferometer measures the return wavefront of light after it is transmitted through a window, is reflected by a flat, and is returned. The return wavefront is the sum of the contri-

Paper 09120 received Dec. 24, 1990; revised manuscript received Feb. 16, 1991; accepted for publication Feb. 16, 1991. This paper was presented at the OSA annual meeting, November 1990, Boston, Massachusetts.
© 1991 Society of Photo-Optical Instrumentation Engineers.

butions of the inhomogeneity of the window material, the figures of both surfaces of the window, and the return flat. Because both surfaces and the return flat are not absolutely flat, the errors due to the surfaces must be removed to determine the inhomogeneity. The procedure, shown in Fig. 1, is as follows:

1. Remove the window and adjust the return flat to obtain a reflection from the return flat C.
2. Insert the window. Adjust the return flat to get a reflection from the return flat C through the window.
3. Measure the wavefront reflected from the front surface A of the window.
4. Adjust the window to obtain the reflection from the rear surface B.

Expressed mathematically,

$$\begin{aligned}
 M_1(x,y) &= 2C + 2S + k_1, \\
 M_2(x,y) &= 2(1 - n_0)A + 2(n_0 - 1)B + 2C \\
 &\quad + 2\Delta + 2S + k_2, \\
 M_3(x,y) &= 2A + 2S + k_3, \\
 M_4(x,y) &= 2(1 - n_0)A + 2n_0B + 2\Delta + 2S + k_4.
 \end{aligned}
 \tag{1}$$

Here M_1 , M_2 , M_3 , and M_4 are the measured wavefronts in each of the above steps; A , B , and C are the surface errors of the front surface, the rear surface, and the return flat, respectively; and Δ is the wavefront deviation due to the inhomogeneity of the window, i.e., material contribution. The average or nominal refractive index is n_0 and $k_{1,4}$ are arbitrary constants because only the relative phase is measured in each measurement. Finally, S is the contribution of the system error. From Eq. (1), multiplying $(M_2 - M_1)$ and $(M_4 - M_3)$ by two factors n_0 and $n_0 - 1$, respectively, then

$$\begin{aligned}
 n_0(M_2 - M_1) - (n_0 - 1)(M_4 - M_3) \\
 &= 2n_0[(n_0 - 1)(B - A) + \Delta] - 2(n_0 - 1) \\
 &\quad \times [n_0(B - A) + \Delta] + \text{constant} \\
 &= 2\Delta + \text{constant}.
 \end{aligned}
 \tag{2}$$

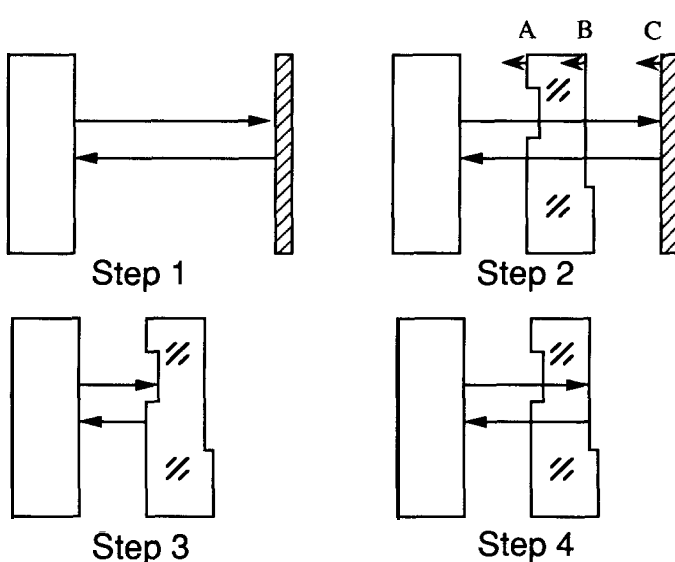


Fig. 1. The measurement procedure for the transmission method.

Therefore,

$$\begin{aligned}
 \Delta(x,y) &= [n_0(M_2 - M_1) - (n_0 - 1) \\
 &\quad \times (M_4 - M_3)]/2 + \text{constant}' .
 \end{aligned}
 \tag{3}$$

Thus the wavefront deviation Δ due to the inhomogeneity can be obtained. When the thickness of the window is given, the variation of the refractive index can be calculated. The constant in the equation affects only the bias of the variation, which is not important with respect to the inhomogeneity. It should be noted that the system error S is eliminated in Eq. (2), in addition to the errors due to the front surface A , the rear surface B , and the return flat C .

2.3. Window-flipping method

The general practice is to measure the two surfaces of the window separately. The front surface is easy to measure. However, for the rear surface, we must flip the window about an axis, e.g., the x axis, and make a measurement, as shown in Fig. 2, step 4'. This requires a flipping mechanism to ensure that the images on the detector overlap before and after flipping the window. After obtaining the measurement wavefront, M'_4 in step 4', we flip M'_4 mathematically about the x axis to obtain \mathbf{M}'_4 . Thus,

$$\begin{aligned}
 M'_4(x,y) &= -2B + 2S + k'_4, \\
 \mathbf{M}'_4(x,y) &= -2B + 2S + k'_4.
 \end{aligned}
 \tag{4}$$

The bold letters denote the transformation of the array flipping 180 degrees about then axis, i.e., $\mathbf{M}'_4(x,y) = M'_4(x,-y)$, $\mathbf{B}(x,y) = B(x,-y)$, and $\mathbf{S}(x,y) = S(x,-y)$. It should be noted that there is a minus sign with B due to the window flipping.

From Eqs. (1) and (4)

$$\begin{aligned}
 M_2 - M_1 + (n_0 - 1)(M_3 + \mathbf{M}'_4) \\
 &= 2[(1 - n_0)(A - B) + \Delta] + 2(n_0 - 1) \\
 &\quad \times [(A - B) + S + \mathbf{S}] + \text{constant} \\
 &= 2\Delta + 2(n_0 - 1)(S + \mathbf{S}) + \text{constant}.
 \end{aligned}
 \tag{5}$$

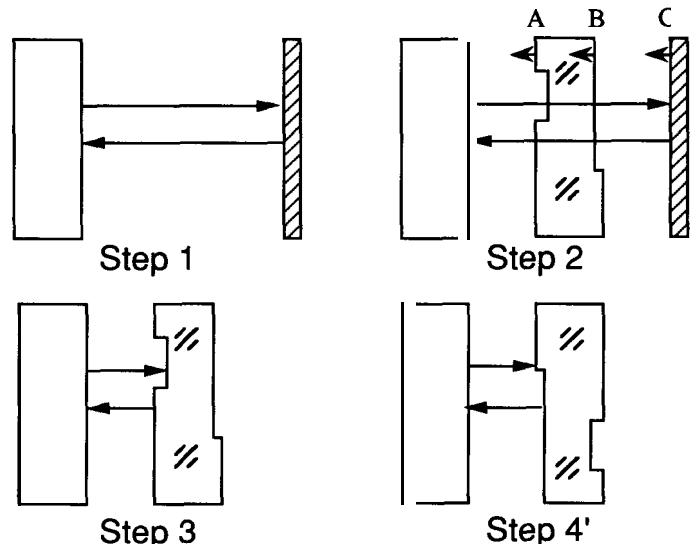


Fig. 2. The measurement procedure using the window flipping method.

Thus,

$$\Delta = [M_2 - M_1 + (n_0 - 1)(M_3 + M_4)]/2 - (n_0 - 1)(S + S) + \text{constant}' \quad (6)$$

It is clear that the system error does not vanish unless it is antisymmetric about the axis of flipping (e.g., the x axis). Because of the window flipping, the system error is not canceled, but can actually increase.

3. EXPERIMENT

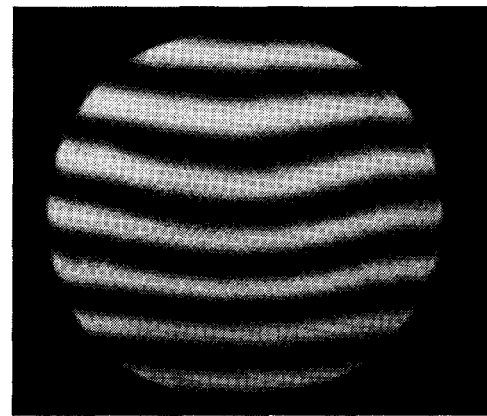
We measured a round window of SFL57, 10 mm thick and 50 mm in diameter, and a rectangular window of BK7, 63 mm long by 38 mm wide by 50 mm thick using a digital interferometer. The windows were measured in the direction along the thickness. The peak-to-valley (p-v) values of the surface figures of both windows are between 0.75 wave and 1.50 waves. Figure 3 shows the interference fringes of the front and the rear surfaces and the return wavefront reflected by the return flat with the SFL57 window. Figures 4(a), 4(b), and 4(c) are the measured inhomogeneity of glass SFL57 obtained with the three methods. The figure clearly shows that there is a delta distribution in the homogeneity. Figure 5 is another measurement result with the transmission method, where the window was rotated by an angle of 30 deg. Mathematically rotating Fig. 5, and comparing it with Fig. 4(a), the difference is 0.010 wave rms, as shown in Fig. 6. Because of the size of the BK7 window, it was not tested with the liquid immersion method. Figures 7(a) and 7(b) show the measured inhomogeneity of glass BK7 with the transmission method and with the window-flipping method. The figure clearly shows that there is a cylindric distribution along the longest dimension in the homogeneity. From Figs. 4 and 7, the wavefront deviations due to the inhomogeneity of SFL57 and BK7 are about 0.75 wave, where the interval cycle of the isometric contour is 0.007 wave. Thus, the variation of the refractive index is about 5×10^{-5} and 1×10^{-5} for SFL57 and BK7, respectively.

Figures 4(a) and 4(b) are very similar to each other, but compared to Fig. 4(c) they have a greater power, i.e., more fringes. The reason why Fig. 4(c) has fewer fringes is that the liquid used in the liquid immersion method has a refractive index approximately equal to 1.785, at 589.3 nm, which does not match that of the window material. Figures 4 and 7 clearly show that there is a delta distribution in the homogeneity in the SFL57 window and a cylindric distribution in the BK7 window. We believe that this delta distribution occurred while the sample was prepared, and that the cylindric distribution occurred in the melting and/or annealing process. Figure 6 is the difference between two measurements; one of them is rotated mathematically. The figure shows the footprint of the three-chuck mount. Thus, the measurement accuracy in this experiment is about 0.010 wave rms, and is limited by the mounting mechanism. If the measurement is performed carefully, 0.005 wave rms can be achieved. The similarity among the results using all three methods shows that the transmission method works very well.

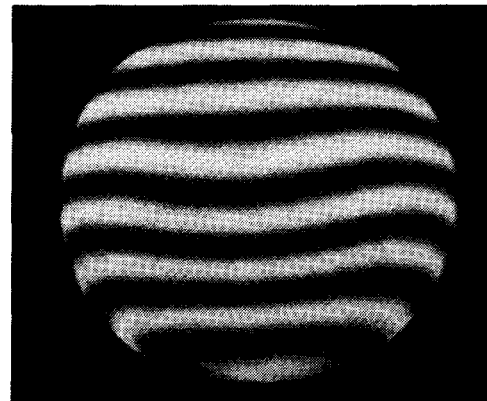
4. DISCUSSION

Here we discuss the error sources and the measurement accuracy. The first error source is the interferometer random noise, as explained below. The contribution of the window to the transmitted wavefront is

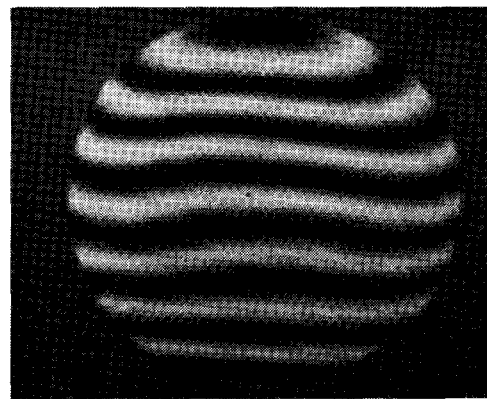
$$\text{OPD}(x,y) = [n(x,y) - 1]T(x,y) \quad (7)$$



(a)



(b)



(c)

Fig. 3. Interference fringes of an SFL57 window. (a) Front surface, (b) rear surface, (c) return wavefront reflected by a return flat.

where $n(x,y)$ is the refractive index, and $T(x,y)$ is the window thickness. Both are functions of x and y . For simplicity, only x is used. Therefore, the variation of the optical path difference (OPD) over the pupil of the window is

$$\begin{aligned} \text{OPD}(x) - \text{OPD}_0 &= [n(x) - 1]T(x) - (n_0 - 1)T_0 \\ &= [n_0 + \eta(x) - 1][T_0 + t(x)] - (n_0 - 1)T_0 \\ &\approx (n_0 - 1)t(x) + T_0 \eta(x) \end{aligned} \quad (8)$$

where n_0 is the average refractive index, T_0 is the nominal or average thickness, and OPD_0 is the average OPD equal to

$(n_0 - 1)T_0$. The refractive index variation $n(x)$ equals $n(x) - n_0$. The thickness variation $t(x)$, equal to $T(x) - T_0$, is equal to the difference of the front and rear surfaces plus the wedge of window, if it exists. However, the effect of the wedge is

equivalent to the tilt of a wavefront, which is not important and usually not measured. Hence, $(n_0 - 1)t(x)$ equals the wavefront deviation due to the thickness variation, and $T_0\eta(x)$ is equal to the wavefront deviation due to the inhomogeneity. In Eq. (8), the cross term, $\eta(x)t(x)$, is dropped because it is too small compared to the other two terms.

From Fig. 1, $M_2(x) - M_1(x)$ equals the contribution from the window. Also, from Eq. (1),

$$\frac{[M_2(x) - M_1(x)]}{2} = (n_0 - 1)[B(x) - A(x)] + \Delta(x) + \text{constant} \quad (9)$$

There is a factor 2 in the denominator, because $M_2(x)$ and $M_1(x)$ are the returned wavefronts, which go through the window and the cavity twice. Comparing Eq. (9) with Eq. (8), we can see that

$$t(x) = B(x) - A(x) \quad ,$$

and (10)

$$\Delta(x) = T_0\eta(x) = T_0[n(x) - n_0] \quad ,$$



(a)



(b)



(c)

Fig. 4. The measured inhomogeneity of glass SFL57 with (a) the transmission method, (b) the window-flipping method, and (c) the liquid immersion method. The interval of the isometric contour is 0.07 wave. (a) p-v = 0.711 wave, rms = 0.166 wave. (b) p-v = 0.793 wave, rms = 0.166 wave. (c) p-v = 0.646 wave, rms = 0.141 wave. The figures clearly show that there is a delta-shaped distribution of the homogeneity.



Fig. 5. The measured inhomogeneity of the SFL57 window with the transmission method where the window was rotated 30 deg. The interval of the isometric contour is 0.07 wave, p-v = 0.725 wave, and rms = 0.164 wave.

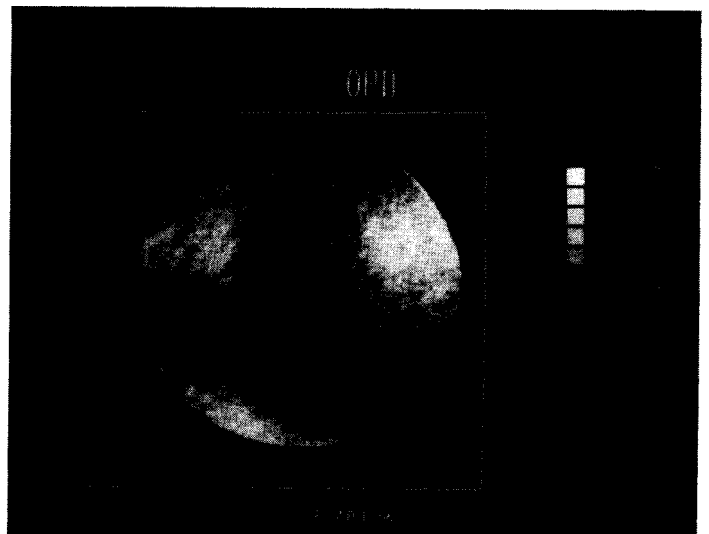


Fig. 6. The difference between Fig. 4(a) and Fig. 5 shows the effect of the three-chuck mount. Figure 5 is mathematically rotated to match the orientation of Fig. 4(a).

where the constant is dropped because only the variation is of interest. Thus the wavefront deviation $A(n)$ due to the inhomogeneity is equal to the refractive index variation $n(x) - n_0$ times the thickness of the window T_0 . If the thickness of the window T_0 is given, from Eq. (10), $n(x) - n_0$ can be obtained as follows:

$$n(x) - n_0 = \Delta(x)/T_0 \quad (11)$$

It is important to know that the peak-to-valley value of Eq. (11) gives the maximum variation of n .

From the right-hand side of Eq. (3), the rms error δ_1 for the measurement of the material contribution due to the random noise is equal to

$$\delta_1 = 0.5\epsilon[2n_0^2 + 2(n_0 - 1)^2]^{1/2} \quad (12)$$

where ϵ is the rms error for a phase measurement due to the random noise, i.e., the repeatability of the interferometer. Thus, for $n_0 = 4$, the rms error is 3.5ϵ , and for $n_0 = 1.6$, the rms error is 1.2ϵ . In Eq. (11), $\Delta(x)/T_0$ determines the refractive index variation. Similarly, δ_1/T_0 gives the measurement accuracy of the refractive index variation. Because δ_1 is limited by the interferometer, the thicker the window, the more accurate the result. Note that Δ and δ_1 in Eqs. (11) and (12) have the same unit of dimension in waves, and that Δ/T_0 and δ_1/T_0 are dimensionless.

For example, a window of $T_0 = 10$ mm and $n_0 = 1.6$ is measured at 633 nm. If the maximum wavefront deviation A due to the inhomogeneity is 0.16 wave, peak to valley, from Eq. (11), the maximum variation of n equals 10×10^{-6} . Typically, glass of good homogeneity⁶ has a maximum variation of n equal to $\pm 5 \times 10^{-6}$, which are the extremes of the refractive index, and whose difference equals 10×10^{-6} . If the interferometer has a repeatability $\epsilon = 0.002$ wave rms, then from

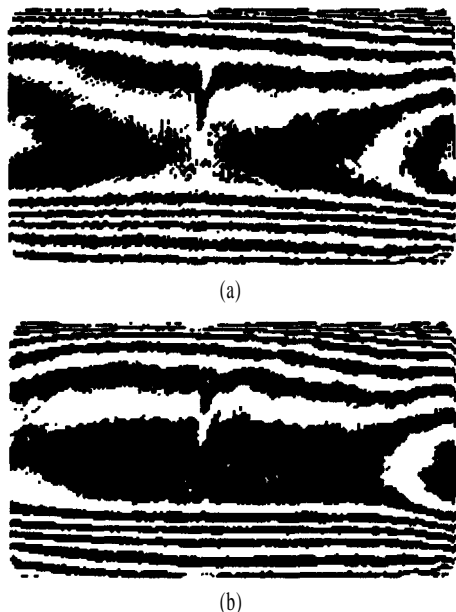


Fig. 7. The measured inhomogeneity of glass BK7 (a) with the transmission method and (b) the window flipping method. The figure clearly shows that there is a cylindrical distribution along the longest dimension in the homogeneity. The interval of the isometric contour is 0.07 wave. (a) p-v = 0.722 wave, rms = 0.118 wave. (b) p-v = 0.715 wave, rms = 0.118 wave.

Eq. (12) the measurement rms error $\delta_1 = 0.0024$ wave, and $\delta_1/T_0 = 0.15 \times 10^{-6}$. Thus, the measurement error is about 1.5%.

Another error source is the error of the refractive index input. In Eq. (2), $(M_2 - M_1)$ and $(M_4 - M_3)$ are multiplied by two factors that are determined by the refractive index. This refractive index usually is the nominal value n_n from a glass catalogue, and is not necessarily equal to the average refractive index of the window material under test. Substitute n_n and $n_n - 1$ for the two factors mentioned above, then

$$\begin{aligned} n_n(M_2 - M_1) - (n_n - 1)(M_4 - M_3) \\ = 2n_n[(n_0 - 1)(B - A) + \Delta] - 2(n_n - 1)[n_0(B - A) \\ + \Delta] + \text{constant} \\ = 2(n_0 - n_n)(B - A) + 2\Delta + \text{constant} \end{aligned} \quad (13)$$

Note that if the refractive index input n_n is not equal to the average refractive index n_0 , then an error occurs. Therefore, the rms error δ_2 for the measurement of the material contribution due to the error of the refractive index input can be expressed as

$$\delta_2 = |n_0 - n_n|(B - A)_{\text{rms}} \quad (14)$$

For instance, if the discrepancy between the refractive index input and the average refractive index $n_0 - n_n = 0.002$, which is the maximum deviation for a melt from the value stated in a glass catalogue,⁶ and the thickness variation $(B - A)_{\text{rms}} = 2$ wave, then δ_2 is about 2.004 wave. For the same example above, $\delta_2/T_0 = 0.25 \times 10^{-6}$. From Eq. (14), the smaller the error of the refractive index input, the smaller the measurement error of the refractive index variation. Note that both δ_1 and δ_2 are independent of the average thickness of window.

The typical and maximum values of the variation of the refractive index and the corresponding errors of the homogeneity measurement are summarized and tabulated in Table 1. In the above experiment, for the SFL57 window that is 10 mm thick, the peak-to-valley value of the wavefront deviation is about 0.75 wave. Thus, the maximum variation of n for SFL57 is about 50×10^{-6} . For the BK7 window that is 50 mm thick, the peak-

Table 1. The typical and maximum values of the variation of the refractive index and their corresponding wavefront deviation and errors of the homogeneity measurement.

	$n_0 - n_n$ ⁽¹⁾	δ_2 ⁽²⁾	δ_1 ⁽³⁾
maximum	± 0.0020	0.040 wave	-----
typical	± 0.0005	0.008 wave	0.0024 wave
	$n(x) - n_0$ ⁽⁴⁾	$\Delta(x)$ ⁽⁵⁾	$\Delta(x)/T_0$
maximum	$2 \times 10^{-4} (= \pm 1 \times 10^{-4})$	3.20 wave	200×10^{-6}
typical	$1 \times 10^{-5} (= \pm 5 \times 10^{-6})$	0.16 wave	10×10^{-6}

$T_0 = 10$ mm, 1 wave = 633 nm.

⁽¹⁾The refractive index deviation for a melt from the value n_n stated in a glass catalogue⁶, where n_n is the average refractive index.

⁽²⁾ δ_2 is due to the error of the input refractive index, where $(B - A)_{\text{rms}} = 2$ waves.

⁽³⁾ δ_1 is due to the interferometer repeatability, and depends on n_0 , not $n_n - n_0$. For $\epsilon = 0.002$ wave rms and $n_0 = 1.6$, from Eq. (12) δ_1 equals 1.2 ϵ .

⁽⁴⁾The degree of the refractive index variation over the pupil.

⁽⁵⁾The peak-to-valley value of the wavefront deviation $\Delta(x)$ due to inhomogeneity for a window 10 mm thick. $\Delta(x) = T_0[n(x) - n_0]$.

to-valley value of the wavefront deviation is also about 0.75 wave. Because the BK7 window is much thicker than the SFL57 window, the maximum variation of n for BK7 is much smaller than that of SFL57, approximately equal to 10×10^{-6} . Therefore, the refractive index of BK7 is much more uniform than that of SFL57. It is obvious but important that the peak-to-valley value of the wavefront deviation is also dependent on the size of the window and not just the thickness. In brief, for the same window material, the larger and thicker the piece, the more difficult it is to obtain a uniform refractive index.

When the window-flipping method is used, from Eq. (6), the two errors mentioned above still exist. Besides those, we see that the system error could contribute the greatest part of the measure error, if $S + S$ is not equal to zero. For the same window of $T_0 = 10$ mm and $n_0 = 1.6$ measured at 633 nm, if the system error $S_{ms} = 0.01$ wave, δ is on the order of 0.01 wave. Thus, $\delta/T_0 = 0.6 \times 10^{-6}$.

5. CONCLUSION

The advantage of the oil immersion method is that the surface only needs to be fine ground. The disadvantage of this method is that the use of a liquid is inconvenient for some applications. It should be noted that the refractive index of oil must be as close as possible to that of the window material. However, oil of a higher refractive index is difficult to obtain.

The two major error sources for the transmission method are the random noise of the interferometer system and the discrepancy between the refractive index input and the refractive index averaged over the pupil of the test window. The contributions of the two error sources have approximately the same magnitude. The contribution from the first error source is linearly proportional to the interferometer repeatability. For the second error source, the resulting error is linearly proportional to the error of the refractive index input. Both error sources are independent of the average window thickness. Therefore, the measurement accuracy of the refractive index variation is inversely proportional to the thickness. Hence, in order to obtain the most accurate measurement, we should use the thickest window plate, the least noisy interferometer, and the best estimated refractive index.

The advantages of this transmission method are as follows: (1) The contributions due to the figure errors of both surfaces of the window, the return flat, and the system error are removed completely. (2) It is easy to mathematically process the data because only the operations of multiplication and differencing are necessary. (3) It is easy to take a measurement because neither a flipping mechanism nor liquid is needed. The disadvantage of this method is that it requires both surfaces to be polished within a few fringes, and a small wedge must be fabricated between the two surfaces to eliminate the spurious interference.

For the window-flipping method, the system error contributes the greatest part of the measurement error, because the system

error is not canceled. The two error sources mentioned above still exist for this method. The advantage of this method is that because the two surfaces are measured in reflection completely independently, the spurious reflection from the back surface can be blocked by spreading a coating on the measured surface. Therefore, it can test a window that has no wedge between the two surfaces.

6. ACKNOWLEDGMENTS

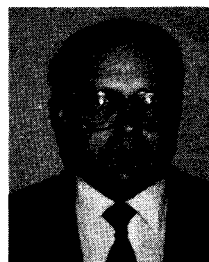
We wish to thank Robert J. Scheller of Schott Glass for providing the sample SFL57 and Philip Lam of Lam Optics for providing the sample BK7.

7. REFERENCES

1. I. Adachi, T. Masuda, and S. Nishiyama, "A testing of optical materials by the Twyman type interferometer," *Atti Fond. Giorgio Ronchi Contrib. Ist. Naz. Ottica*, 16, 666-674 (1961).
2. M. V. R. K. Murty, "Newton, Fizeau, and Haidinger interferometers," in *Optical Shop Testing*, Daniel Malacara, ed., pp. 1-45, John Wiley and Sons, New York (1978).
3. F. Twyman and J. W. Perry, "Measuring small differences of refractive index," *Proc. Phys. Soc. London* 34, 151 (1922).
4. F. E. Roberts and P. Langenbeck, "Homogeneity evaluation of very large disks," *Appl. Opt.* 8(11), 2311-2314 (1969).
5. J. Schwider, R. Burow, K.-E. Ellsner, R. Spolaczyk, and J. Grzanna, "Homogeneity testing by phase sampling interferometry," *Appl. Opt.* 24(18), 3059-3061 (1985).
6. "Definition of quality," in *Optical Glass*, pp. 37-39, Schott Glass Tech. Inc., Duryea, Pennsylvania.



Chiayu Ai received his BS in physics in 1975 from the National Taiwan Normal University, his MS in physics in 1978 from the National Tsinghua University, and his Ph.D. in optics in 1987 from the University of Arizona. He has been employed as an Optical Engineer at WYKO Corporation since his graduation in 1987, and is responsible for the development of optical testing systems.



James C. Wyant received his BS in physics in 1965 from Case Western Reserve University and MS and Ph.D. degrees in optics from the University of Rochester in 1967 and 1968. He was an optical engineer with Itek Corporation from 1968 to 1974, when he joined the faculty of the Optical Sciences Center at the University of Arizona, where he is now a professor of Optical Sciences. He is President of the WYKO Corporation. Wyant has published more than 100 papers in the areas of holography, interferometry, and optical testing, and he is a coeditor of the book series, *Applied Optics and Optical Engineering*. He is a former member of the Board of Directors and Executive Committee of the Optical Society of America and he is a past president of SPIE.